The International Journal of Advanced Manufacturing Technology (2022) 120:4233–4270
https://doi.org/10.1007/s00170-022-09021-6

CRITICAL REVIEW

A review on peening processes and its effect on surfaces

Syed Qutaba[1,4] · Mebrahitom Asmelash[2] · Kushendarsyah Saptaji[3] · Azmir Azhari[1]

Received: 7 October 2021 / Accepted: 6 March 2022 / Published online: 18 March 2022

Abstract
Surface treatment methods are widely used in various industries to improve the material performance and change their physical properties. The methods can be categorised according to the nature of the operation as mechanical, chemical, electrochemical and case hardening processes. Mechanical surface treatment methods are mainly utilised to add compressive residual stresses in surface layers thus usually improving the life of engineering components. Among various mechanical surface treatment methods, peening process is common in treatment nature by treating the surface using mechanical means. Three peening processes, namely shot peening (SP), laser shock peening (LSP) and waterjet peening (WJP) are selected to be the focus of the present paper due to their similarity based on impulsive effect to the surface by the input force through unguided tools in repetitive irregular manner without any oscillating or vibrating movement of tools. A comprehensive review is presented to discuss each of the peening processes and their effects on the surface integrity in terms of the topography, mechanical properties and microstructural changes. The investigation includes the discussion on the existing advantages, disadvantages and technological barriers of peening technologies for industrial applications. Detailed examples of recent advances in the peening methods are also discussed. The results show that the SP method produces more roughness as compared to LSP and WJP methods. However, fatigue strength is better without considerable changes in roughness and corrosion after LSP and WJP treatments. It can be concluded that the peening processes can improve the material performance with acceptable qualities for in-service application in industries.

Keywords Surface treatment · Peening processes · Metallic surfaces · Topography · Metallurgical states · Surface integrity · Fatigue growth · Corrosion

1 Introduction

Surface treatment technologies have become more important in the industry to reduce the economic costs and avoid the need for expensive materials. The surface treatment has a long history from various applications but it is highly involved in the mechanical industry since 30 years ago [1, 2]. The material surface influences the performance of engineering parts, which are often exposed to different surface treatment processes in order to obtain values not achievable from primary manufacturing processes [3]. The process is carried out for a variety of reasons, including improving the material performance, changing physical properties, appearance and altering dimensions [4].

Figure 1 shows the classification of surface treatment processes. It can be categorised according to the nature of the operation as mechanical, chemical, electrochemical and case hardening process. Mechanical surface treatments can be divided into two categories which are hot processes such as rolling, welding and laser shock peening (LSP) as well as cold processes such as hammering, cold rolling, shot peening (SP) and waterjet peening (WJP). These processes are utilised to add compressive residual stresses (CRS) in surface layers, which typically bring about critical life improvement [5]. In chemical processes, there are many popular surface treatment processes used in daily life like hydrolysis, acid etching, immersion and coating, which can

✉ Syed Qutaba
engrsyedqutaba@gmail.com

1 Faculty of Manufacturing and Mechatronics Engineering Technology, Universiti Malaysia Pahang, 26600 Pekan, Pahang, Malaysia

2 College of Engineering, Universiti Malaysia Pahang, 26300 Gambang, Pahang, Malaysia

3 Department of Mechanical Engineering, Faculty of Engineering and Technology, Sampoerna University, Jakarta, Indonesia

4 Department of Textile, BUITEMS, Quetta 87100, Pakistan

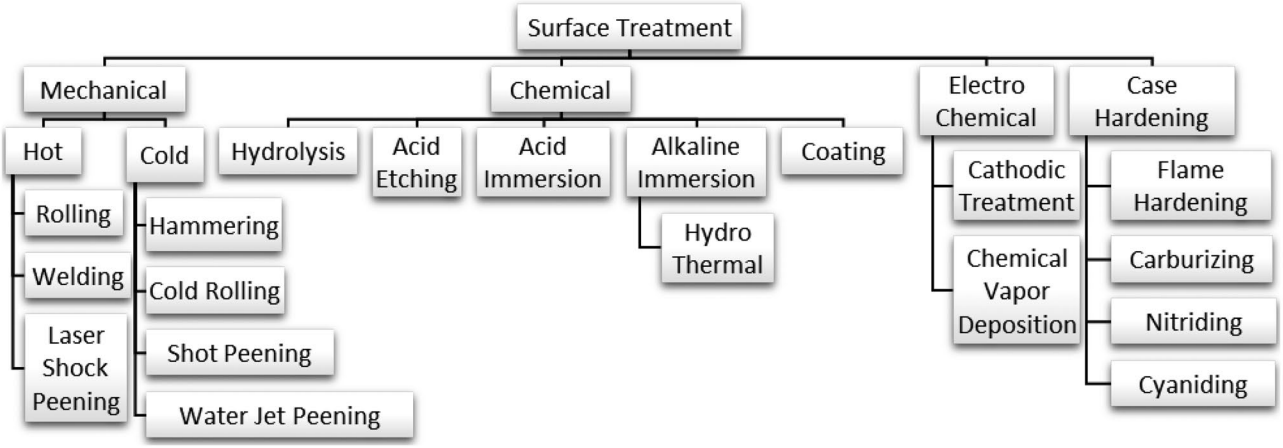

Fig. 1 Classification of surface treatment process

improve the surface layers properties. Furthermore, examples of processes under the combination of electrical and chemical operation or electrochemical are cathodic treatment and chemical vapour deposition (CVD). Finally, case hardening processes such as flame hardening, carburizing, nitriding and cyaniding use heat during the treatment which can improve the surface layer properties like smoothness, roughness and hardness [6, 7].

A variety of heat and mechanical treatments have been used for a broad variety of the substrate, including semiconductors, metals, ceramics, polymers, bio and nanomaterials, to alter surface characteristics [8]. The surface treatment sub process has linked with the other methods like chemical and electro-chemical for changing chemical properties of surface as well as chemical routes for depositing particles and coatings which are exits [9]. The improvement of surface area is usually adjusted for effective surface area using sandblasting (SB), SP or LSP methods thus achieving mechanical retention between two surfaces [10]. Such adjustments and modifications of this nature may have varying levels of flexibility and are usually alienated into the two divisions: surface concave texturing and surface convex texturing as shown in Fig. 2a [11]. Chemical or electrochemical layer removal or mechanical indentations (caused by SB, SP or LSP) may be used to create surface concave textures [12].

The favourable compressive residual stress can be fabricated at the surface dependent on blasting/peening operating situations (counting media size, arc-heights and coverage). Surface convex textures, on the other hand, might be well formed by putting different sorts of the particles using one of several physical or chemical depositing methods (chemical vapour deposition, physical vapour deposition, plasma-spraying, etc.) or solid-state diffusion bonding [13].

The surface requirements primarily determine the type of materials and manufacturing methods to be used during the production process. Surface properties do not only necessitate specific production sequences, but they also influence the layout and geometry of the component. Figure 2b shows the product functionality as well as the haptic properties (with respect to the value perception of the product) and appearance [10]. The components whether it is metal or non-metal, created by three classification states which are

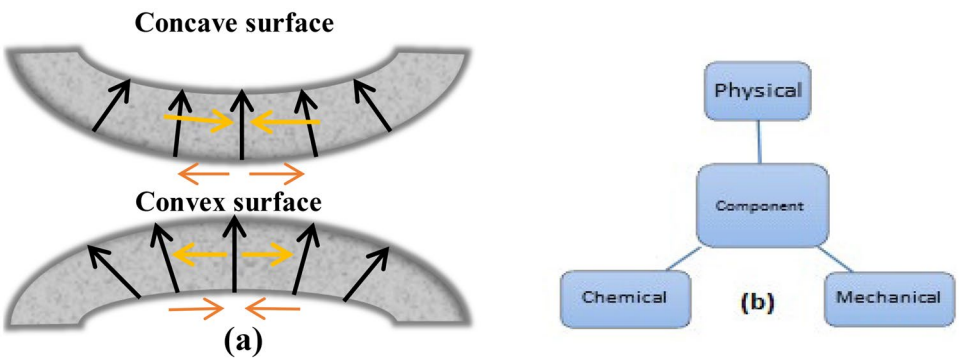

Fig. 2 **a** Surface classification [11] and **b** composition of component

categorised as physical, chemical and mechanical. These classifications are further responsible for their properties and other aspects [2].

It can be noted that surface treatment methods are too diverse covering different aspects and nature of the process. The scope of the present paper will be too wide if all methods are covered. Therefore, the present paper only focuses on mechanical surface treatment methods. This is due to the fact that nowadays, mechanical surface treatments have been widely applied particularly in the spring-manufacturing, automotive and aerospace industries. Furthermore, these processes are known to be well established in ancient times concerning metallic materials where evidently hammering was the first mechanical method used to make particular components to final shape and strength [14]. There are many industrial applications involving mechanical surface treatment methods because of low operating cost, mass production (e.g. rolling), good and acceptable quality of treated products.

As presented in Fig. 1, there are several methods available in mechanical surface treatment. The present review paper will be very long if all methods are to be reviewed thoroughly. Therefore, there is a need to focus on very few methods in mechanical surface treatment which are common in treatment nature. Peening processes, namely shot peening (SP), laser shock peening (LSP) and waterjet peening (WJP) are selected to be the focus of the present paper. In principle, they have similarity in terms of their treatment nature which is based on impulsive effect to the surface by the input force. Furthermore, they use unguided tools in repetitive irregular manner without any oscillating or vibrating movement of tools [15, 16]. Also, the input force is repetitive in nature which impacts the surface (i.e. ball shots in SP, laser beam in LSP, waterjet in WJP). Furthermore, peening processes are considered modern mechanical surface treatment methods which have been started within the last century. Among various peening processes, shot peening (SP) and laser shock peening (LSP) have been widely used in many industrial applications for treatment of automotive and aerospace components [17]. Where, waterjet peening (WJP) has attracted increasing attention among researchers in the last decades [18]. Therefore, it is crucial to provide necessary details related to these peening processes. The present paper discusses a thorough and critical review of the existing literature on the working principles of SP, LSP and WJP processes and their effects on surface integrity of metals.

This review paper is divided into several sections. Firstly, a section discusses the mechanical surface treatment methods for both hot and cold types. Typical processes for hot (e.g. rolling) and cold treatment (e.g. hammering) are explained in detail. Then, another section describes the surface integrity in general. This includes the aspects of surface and sub-surface covering its topography, mechanical properties and metallurgical states. Subsequent sections discuss thoroughly about each of peening processes, namely SP, LSP and WJP. Working principles and major contributions by researchers from each process are elaborated. Also, some new developments in each process to improve the treatment procedures and the quality of treated surfaces are included. Finally, the comparison of all three peening processes is presented in terms of their advantages and limitations. It is hoped that the present paper can shed some light on the applications of various peening processes in mechanical surface treatment methods and their effects on metallic surfaces. Researchers and practitioners can articulate based on the information provided for further improvement and optimisation of the process in widening its application in related industries.

2 Mechanical surface treatment process

Various mechanical treatment processes can be applied to enhance the surface characteristics of engineering components. These treatments use physical processes to determine the resulting surface condition. The compressive stresses are mainly induced into ductile metals mechanically by localised plastic deformation within the outer surface region. The present study is confined to describing the non-cutting methods which serve to primarily enhance the surface layer state. There are two types of mechanical surface treatment processes which exist in industry, namely hot and cold. The hot mechanical surface treatment uses thermal energy like heat or emits energy sources on secondary surfaces to improve the main surface layers like the rolling process. Whereas, the cold surface treatment process uses the secondary material to treat the main surface layer thus increasing the mechanical properties of the surface. In this treatment process, any cold secondary material can strike the main surface layer and improve their mechanical properties such as hardness and roughness.

2.1 Hot mechanical surface treatment process

An example of hot mechanical surface treatment processes is surface rolling. It is a metal shaping interaction where metal stock is gone through at least one set of moves to lessen thickness, uniform thickness, or potentially give an ideal mechanical property on the surface [5]. Surface rolling is graded according to the temperature of the rolled metals [19]. The method is known as hot rolling when the temperature of the metal is higher than its recrystallization temperature [20].

Various factors such as reheating conditions, in-line scale removal, rolling temperature and cooling rate may influence the type and thickness of scale formed on the

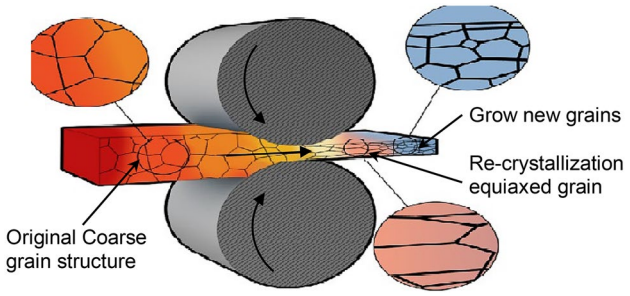

Fig. 3 Schematic view of hot surface rolling process [22]

product, which affects the atmospheric corrosion, paint ability and subsequent scale-removal operations [21]. Figure 3 shows the hot rolling process where the final pass may generate specific surface patterns, such as protrusions on reinforcing bars or floor plates. Whereas, in cold-surface rolling, a particular surface roughness is trolled into the stripe at the temper mill to improve the deep-drawing process and ensure a good surface finish on the final product, decent surface completion on the end result, like the top of an automobile.

Another process of hot mechanical surface treatment is welding. It is a technique for joining metallic parts that typically involves the use of heat. This technique was discovered while attempting to shape iron into useful shapes [23]. Welded blades were invented in the first millennium CE, with the most famous examples being those made by Arab armourers in Damascus, Syria [24].

2.2 Cold mechanical surface treatment process

Hammering is an example of a cold mechanical surface treatment process. A hammer is a tool used to strike the alternative piece or material, such as wood, metal, stone or anything else as shown in Fig. 4. Recently, the concept

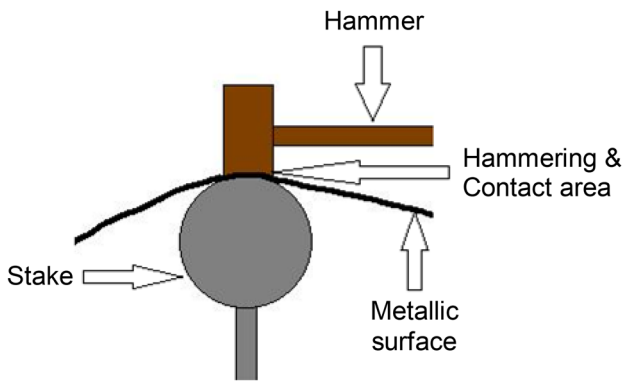

Fig. 4 Hammer peening process

of peening process is applied in hammering to introduce a novel technology in surface treatment called machine hammer peening (MHP) [15]. In this process, a hammering tip is attached to an oscillating plunger which moves axially by an actuator thus providing uniform impact intensity across the machined area [15]. Chan and Cheng [25] discussed comprehensively how hammer peening has evolved into its current state today and its role in various industries.

Surface rolling is also applied without the use of heat during the cold mechanical surface treatment process. In the process, a sheet metal or strip stock is passed between rollers before being compressed and squeezed as shown in Fig. 5. The hardness and other material properties of the finalised product are influenced by the size of strain produced. The benefits of cold surface rolling include excellent dimensional consistency and a smooth finish at the surface [5].

2.3 Recent mechanical surface treatments

The most recent mechanical surface treatments nowadays are shot peening (SP), laser shock peening (LSP) and the latest one is waterjet peening (WJP). These peening processes especially SP and LSP are widely used in industry to create a compressive residual stress speciality in the substrate layer of a metallic element [26, 27]. The first patent for SP was also issued in Germany in 1934, but it was never commercialised, but the automotive industry later adopted this procedure [28]. This technique is used for increasing the fatigue life of the metallic component by delaying crack initiation or smoothing the crack propagation rate [29].

Recent advancement of surface treatment in the LSP process gives better results on material properties such as surface hardness, fatigue life and resistance to corrosion by imparting beneficial residual stresses in materials [28]. When the laser beam of high intensity comes to contact a sample surface, the expansion of laser-induced plasma close to the surface generates a strong shock wave into the sample [8].

In the last two decades, WJP technique has gained popularity in the mechanical surface treatment industry. In comparison with the previous peening process, WJP is good in corrosion resistance, process control and improvement of the fatigue strength [30]. The advantage of the process is to cover full area with pliability in treating complex area and provide an eco-friendly environment with water jet abrasion that is the principle of process [31].

3 Surface integrity

The surface integrity of materials plays an important role in the response of the engineering components. Surfaces are often subjected to various additional treatments or processes

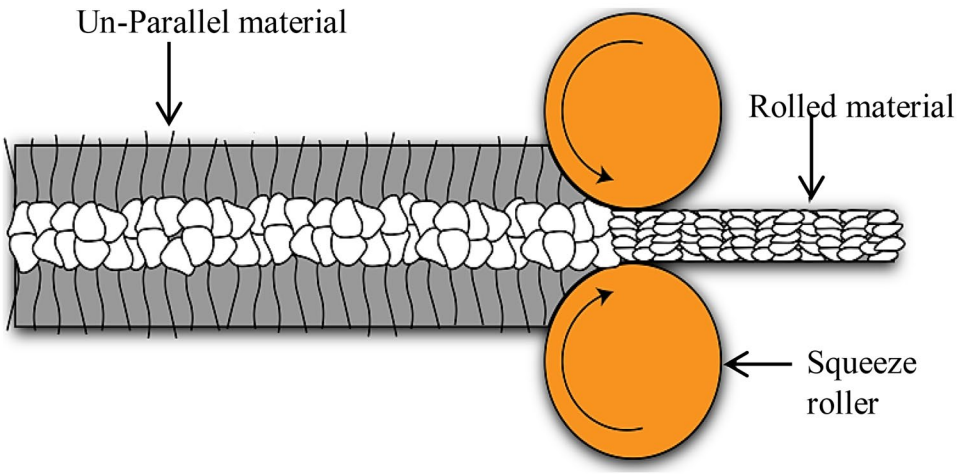

Fig. 5 Schematic view of Surface rolling process

to achieve desirable qualities that are not achieved by primary manufacturing processes. The process is conducted for various reasons including to improve the performance of materials, to change physical properties, to vary the appearance and to alter dimensions. The quality and performance of a product are directly related to its surface integrity produced from different surface treatment or processes. Figure 6 shows the classification of surface integrity that includes the topography which can be analysed such as roughness and waviness, the mechanical properties such as hardness and fatigue strength and the microstructural changes such as phase transformation and microstructures and other related property variations of the work material during surface processing procedures [6, 13]. Therefore, alteration of the surface integrity especially related with mechanical applications has a significant effect on fatigue strength and lifetime of engineering components [20]. Different mechanical treatment methods can be applied to upgrade the surface attributes of engineering parts [32]. These surface treatments utilise some stages to decide the subsequent substrate situation [33]. The localised plastic deformation in the outer surface layer is primarily responsible for compressive stresses in ductile metals [34, 35].

3.1 Topography

The surface topography is defined by the deviation of a surface from its mean plane. It is thought to be an irregular interaction, which is portrayed by the factual boundaries like the fluctuation of the height, the incline and the curve [36]. It can be characterised in several categories such as waviness and roughness. The topography can notably affect the fatigue resistance and strength of load bound and load free surfaces by roughness [37]. Figure 7 shows the indication of surface topography according to different scales, namely macro, micro, nano and their common features. In the case of load-free surface, high roughness is a source for miniature pressure fixation which prompts a deficiency of the fatigue resistance and strength [38]. The need for good surface topography with low roughness is impacted by the machining interaction [39].

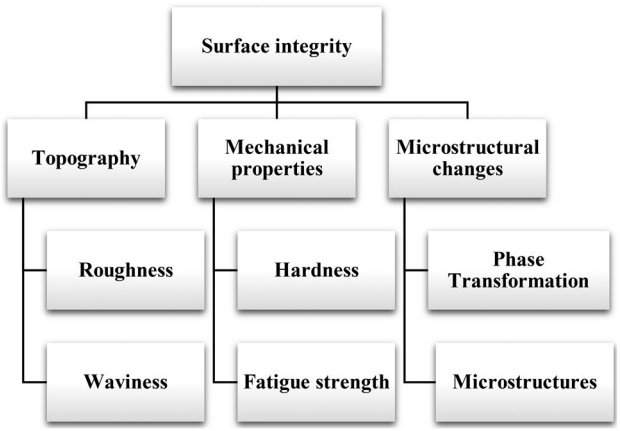

Fig. 6 Classification of surface integrity

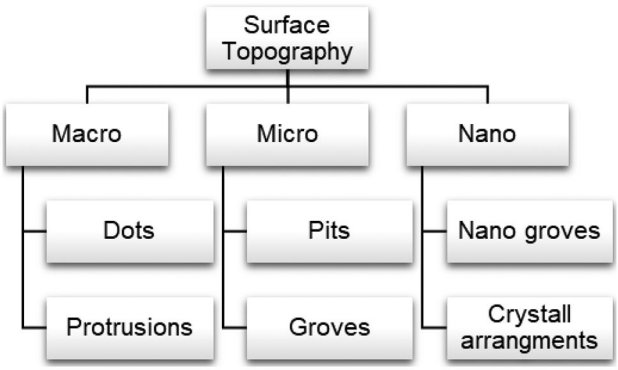

Fig. 7 Surface topography of metallic

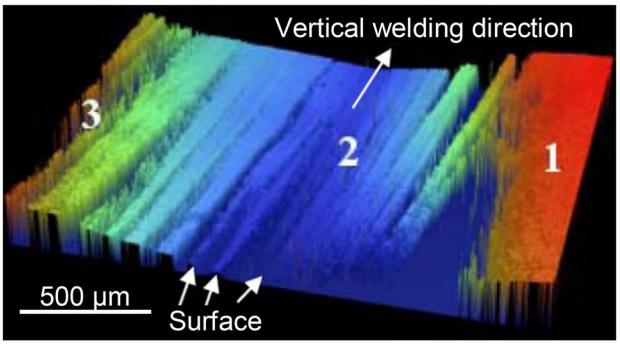

Fig. 8 Ordinary weld surface topography, which is extending from the base metal to the top metal. The ripples run from the base metal (1) to the lower toe (2) to the weld bead (3) [36]

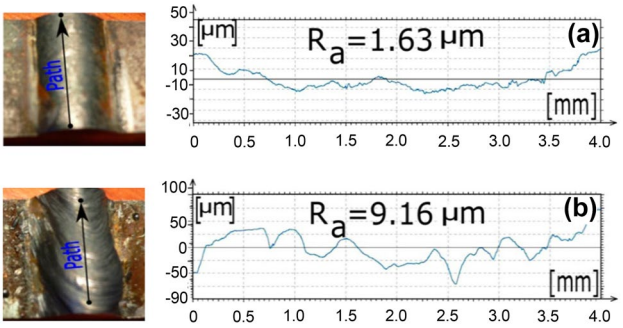

Fig. 9 Roughness profile obtained and paths **a** low values of roughness obtained and **b** high values of roughness obtained [41]

Figure 8 shows an example of welded material with indication of melded toe and their 3D topography. A normal topography scan was taken from the lower toe, which shows the re-solidification patterns covering the upper surface. Apart from the toe radii macro-geometry, the influence of topography (micro-geometry) is supposed to be significant. The larger welding flaws, such as cracks or cold laps, were absent from the surface [36]. Owing to the surface ripples, the roughness was found approximately $R_t = 253.44$ µm and $R_z = 200.35$ µm across and along the weld direction, respectively [36]. This indicates that the welding process can produce a very rough surface to the weld material due to the ripples.

In general, various manufacturing processes including machining, welding and casting will significantly alter the topography of metallic surfaces. There as the effect of surface topography varies according to the peening processes. In LSP, there is practically no surface topography alteration since spots have been enormous (1 to 3 mm) and the profundity of the indent is several 10th of micrometres. In SP, on the contrary, every pit is quite much deeper depending on its processing parameters [33]. When the comparison is made on the traditional mechanical surface reinforcement treatments like SP and cold rolling, there is no major change in topography caused by water jet peening [40].

In a welding process, at the face of each bead, the roughness of the welded joints was determined longitudinally. The face of the weld bead as seen in Fig. 9b has a higher amount of wave than those seen in Fig. 9a, resulting in higher roughness values [41]. This shows that the roughness of weld beads depends on its topography resulting from different welding parameters.

Erosion corrosion is commonly found in components subject to a high-velocity flow of moderately corrosive fluids containing small quantities of solids in suspension [42]. The appearance of the erosion corrosion damaged surface often is smooth, sometimes showing grooves oriented in the direction of fluid flow. Figure 10 shows an example of erosion corrosion signs of a centrifugal pump casing.

3.2 Mechanical properties

There are many important mechanical properties of material that will affect the performance of an engineering component. Among those common properties are hardness, strength, toughness and ductility. The effect of these properties is further discussed in the present work.

Hardness is the most common measurement to determine a change in mechanical properties during mechanical surface treatment methods due to its testing simplicity and low cost. It is defined as the ability of a material to withstand permanent shape change due to external stress [44]. It is characterised by a material's ability to withstand different types of deformation, indentation and penetration, as well as its resistance to scratching, grinding, drilling and chipping to wear and tear [21]. For example, in the case of a

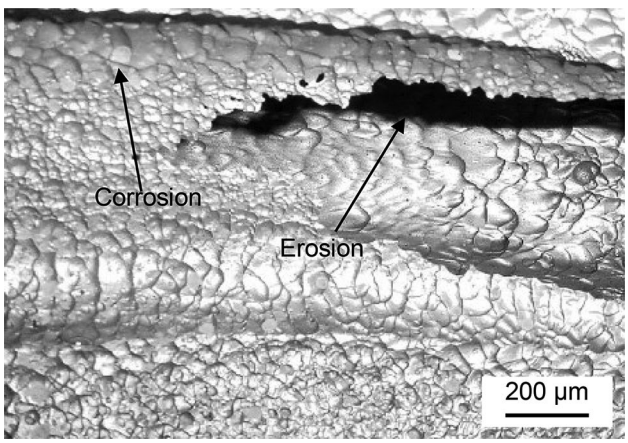

Fig. 10 Erosion and corrosion on the welded fuel pipe [43]

welding process, a higher hardness of the surface with a deeper hardening layer can be achieved by the application of high pressure with an increase in the number of passes [45]. Furthermore, the rolled steel CR690 component hardness changes according to the distance and position of the weld as shown in Table 1.

A higher hardness is produced with an initial increase of distance from the surface. This hardened layer is a result of severe plastic deformation on the surface due the rolling process thus generating compressive residual stresses [45]. The hardened layer and induced compressive residual stresses are useful in avoiding the initiation of crack on the metal surface [46–48]. After that, due to the undue heat, stiffness tends to deteriorate, resulting in the cracking of the surface layer [21]. However, the material hardness is reduced with a further increase in the distance [49].

The tension from a material shortening in one dimension is a result of opposing collinear forces that appear to crush it. Residual stresses persist in an object especially a welded component even when external loading or thermal gradients are absent [1]. Residual stresses can cause severe plastic deformation, resulting in object warping and distortion, and they can also affect fracture and fatigue susceptibility [35, 35]. Figure 11 shows the relationship between the distance from centre and residual stress of VR690 welded joints. The distance of the centre is directly proportional to the residual stresses of the material [45].

3.3 Microstructural changes

The microstructures of a material will change under any mechanical surface treatment methods. These microstructural changes depend on the type of processes and their parameters. Microstructures are tiny scale structures of the material as revealed by a microscope [50]. Microstructures affect various mechanical properties like ductility, toughness

Table 1 Effect of distance and position of welded material on CR690 joints hardness [45]

Position	Distance (mm)	Average hardness (H_V)
Cap of the weld	0	250
	20	350
	40	300
Middle of the weld	0	280
	20	320
	40	310
Root of the weld	0	280
	20	260
	40	270

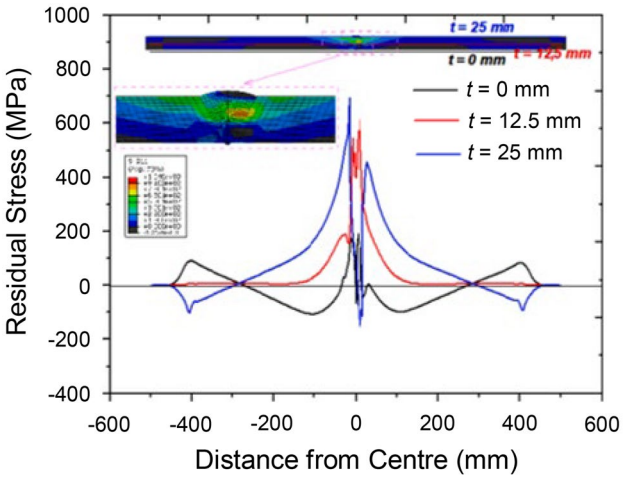

Fig. 11 Effect of distance of depth on residual stress of VR690 welded joint [45]

and hardness. When heat is involved, the microstructures of metal change in stages under a phase transformation process [51]. Most phase transformations do not occur instantaneously; they begin by the formation of numerous small particles of the new phase, which increase in size until the transformation has reached completion [29]. Figure 12 shows an example of a phase transformation cycle commonly occurring in steel during surface treatment processes. In the process, the metal surface experiences a severe plastic deformation thus inducing the phase transformation from the austenite to the martensite [52]. An increase in temperature during the process may further deform the martensite hence reversing it to become austenite [53].

The metals and alloys are made up of several irregularly formed crystals (grains) that are normally undetectable to

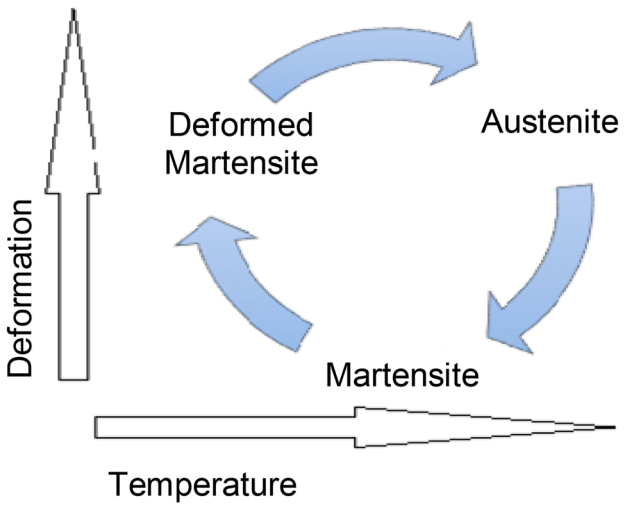

Fig. 12 Cycle of phase transformation

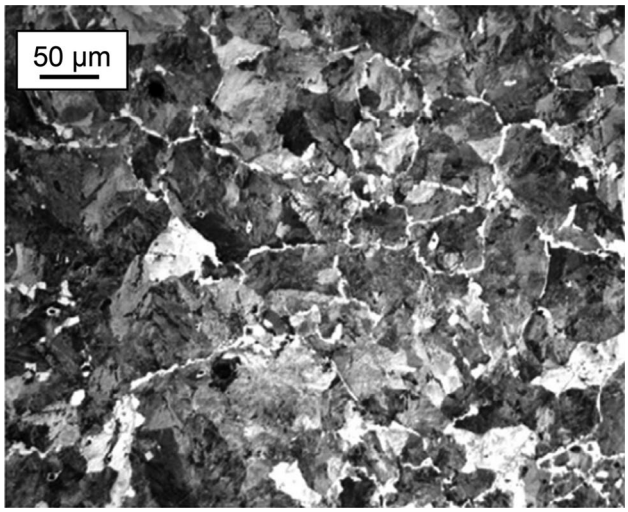

Fig. 13 Microstructure of untreated micro alloyed steel in longitudinal cross section [56]

the naked eye [24]. The grains may be oval or elongated, huge or tiny, either in a regular or random pattern [54]. The shape, size, arrangement and orientation of the grains are all determined by the circumstances under which they were formed. For steel with up to 2.14% weight of carbon content, the microstructure was basically pearlite, ferrite and partially continuous as seen in Fig. 13. Grains are highly equiaxed in both longitudinal and transverse directions. These equiaxed grains may undergo deformation during the surface treatment process thus changing its mechanical properties. For example, during a forging process, the homogenisation leads to an isotropic structure [55].

Another example of phase transformation occurring during the SP process is shown in Fig. 14. Microstructure of untreated high strength steel shows the lath martensitic as shown Fig. 14a. The image of untreated specimen under transmission electron microscope (TEM) evidently shows a smooth and clear boundary of lath martensite as shown in Fig. 14b. After the SP process, the lath martensitic boundary distorts and becomes vague with a significant number of dislocations formed both within and outside the martensitic as shown in Fig. 14c. The dislocations appear to collide with one another and pile up in front of boundaries thus forming a dislocation tangle as it progresses [24].

4 Shot peening

The shot peening process is utilised to increase the surface hardness of metallic materials by inducing compressive residual stress from the ball impact on the material surface [33]. It is a cold working process in which small balls are bombarded by a jet of compressed air onto the surface, and during the process of shot peening, each ball landing on the metallic surface acts like a small hammer, raising its hardness and forming a small indentation or semi-sphere [20]. The small balls or micro shots are usually made from hard materials such as steel, ceramic or glass. The metal surface must be subjected to its yield stress in order to produce these indents, and the overlapping of indentations results in a uniform layer of compressive residual stress on the metal surface thus increasing its resistance to fatigue failure [35].

4.1 Working principle of shot peening

There are two types of shot peening process which exist in industry, namely pneumatic and centrifugal shot peening machines. The working principle of both machines is illustrated in Fig. 15.

Micro shots are combined with compressed volume, simple air and propelled into a nozzle at maximum velocity in the pneumatic shot peening machine as shown in Fig. 15a. In the centrifugal shot peening machine, the shot is pumped into the hub of a spinning wheel with circular vanes or blades as shown in Fig. 15b. In the scenario, the microspheres shot have aimed onto the blades, where centrifugal force causes it to be tossed into a circular rotating-shaped stream. It is clear from the schematic diagrams of both systems that the contact conditions are different thus giving a greater tangential contact force and a higher friction force from the wheel machine [57]. Figure 16 shows the schematic view of the compressive stress development on the peened surface. It can be seen that the impact from the shot causes surface compression which changes the topography and metallurgical state of the workpiece thus altering its mechanical properties [51].

Shot peening process is influenced by several parameters. The typical parameters and their levels are illustrated in Fig. 17 [57, 58].

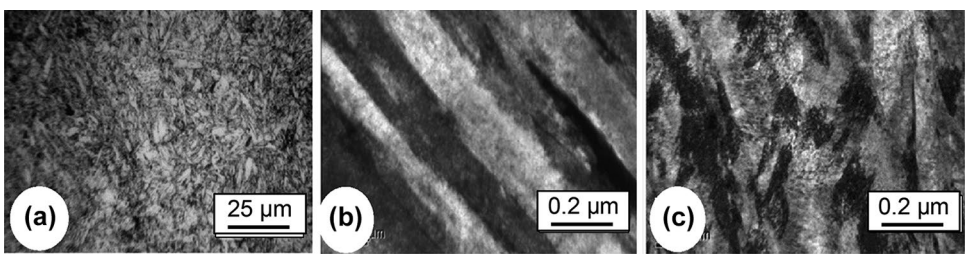

Fig. 14 **a** Microstructure of unpeened high strength steel, TEM images of **b** unpeened and **c** shot-peened specimens [24]

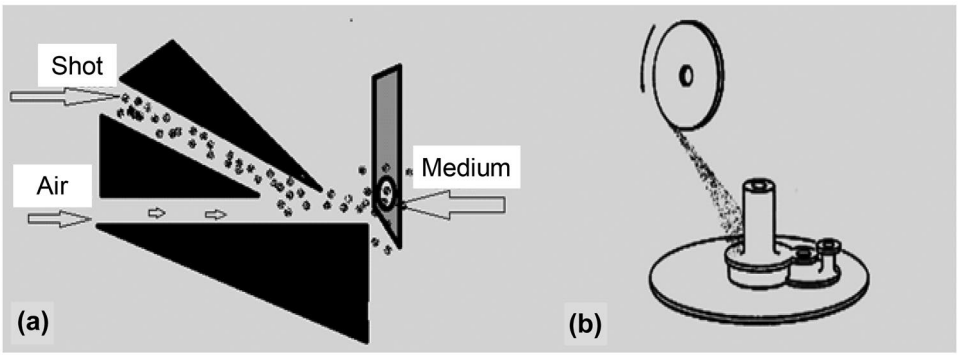

Fig. 15 Schematic view of **a** pneumatic shot peening **b** centrifugal shot peening

In the shot peening process, the kinetic energy transferred by a shot stream is an important factor in determining the quality of peened surfaces. It can be measured using a standard procedure called the Almen Intensity Test developed and patented by John O. Almen [17]. The intensity can be determined by exposing the Almen strip to the shot stream for a specified time as illustrated in Fig. 18a. The strip bends due to the plastic deformations induced by the shot peening. Then, the strip is removed and placed on the Almen gauge as shown in Fig. 18b. The value of the arc deflection at the centre of the Almen strip is recorded as the Almen intensity. A higher intensity (i.e. higher arc deflection) means that a higher amount of kinetic energy has been transferred to the treated components [59]. The Almen strips are made from cold-rolled spring steel (SAE 1070) in three different thicknesses and denoted as *N*, *A* and *C* strips for different intensity measurement levels but all have the same dimensions [17].

4.2 Effect of shot peening on metallic surface

Shot peening is a technique used to improve the fatigue strength of metallic materials, which can result in increased life span, resistance to alternating loads and corrosion resistance [61]. However, the shot peening method has shown no major increases in corrosion resistance [28]. SP produces roughness on the surface [1]. Hardness has affected the increase in peening time [21]. Overall, SP is a stochastic process in which each region must be stroked 13 times on average to reach 100% coverage as compared to LSP which only needs one or two beams (assuming square beam) [20]. Plastic deformation of metal produces residual stresses in the SP process, which persist until it is removed by the external force [62].

4.2.1 Effect of shot peening on topography of metallic surface

The overall enhancements can be measured after a progression of mechanical testing relying upon the application, such as fatigue tolerance, stress corrosion cracking and water erosion resistance, depending on the application. The induced compressive residual stress field and modified microstructures could significantly improve the efficiency of shot-peened layers, such as stress corrosion property and micro hardness [36].

Roughness has increased by the Almen intensity of the treatments when using the cut wire steel shots [63]. However, with the same strength and coverage (8A, 100%), a substantial variation in roughness was found between the steel and ceramic beads (ZS) thus resulting in a significantly lower average in overall roughness values. The shape and homogeneity of the zirconia shots were mainly responsible for these effects. However, using the same ceramic shots, raising the degree of coverage from 100 to 200% resulted in an improvement in the roughness parameters [63]. However, roughness is not an absolute indicator to detect surface flaws like folds and minor fractures which are very common in shot peening treatment [64, 66]. During the SP process, the shots hit the surface thus producing random indents and

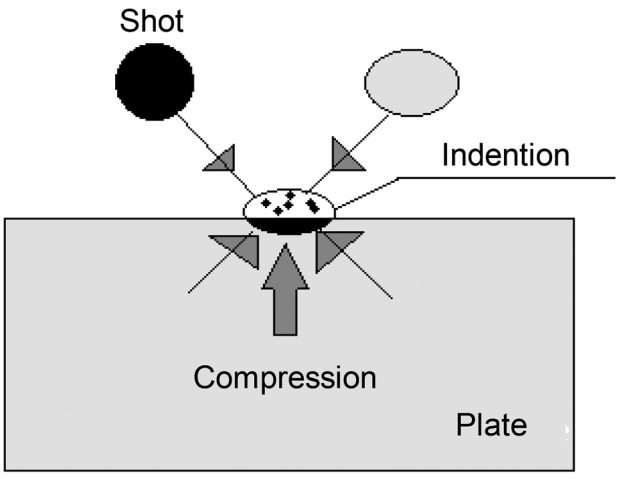

Fig. 16 Schematic view of compressive stresses development on peened surface

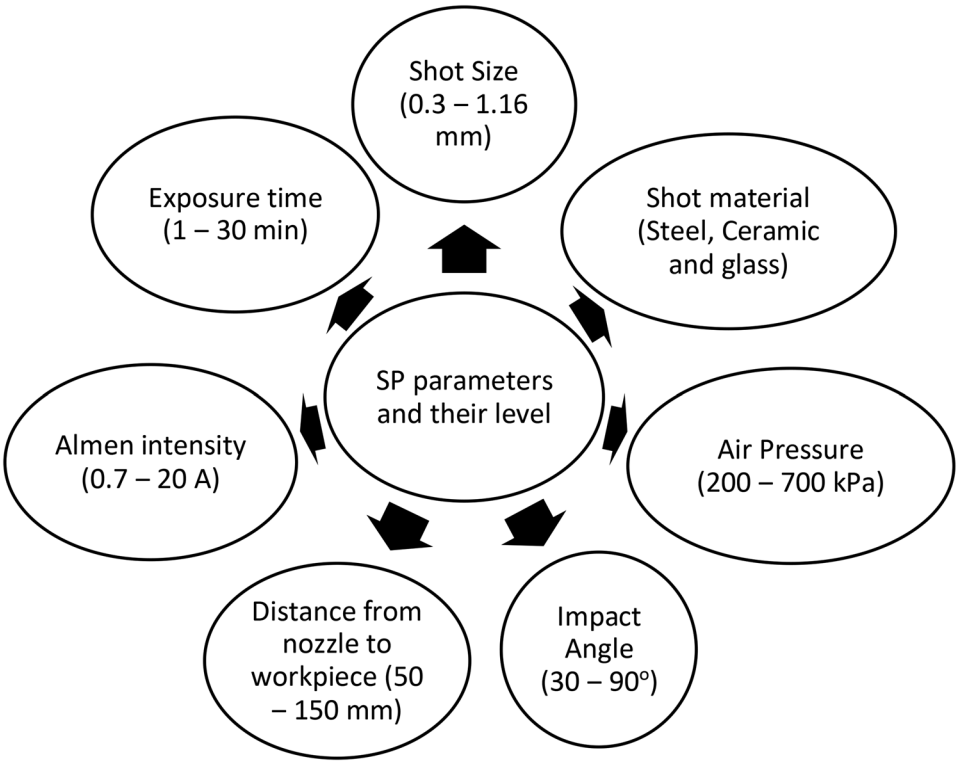

Fig. 17 Typical shot peening parameters and their levels

leaving scattered nodes. Figure 19 shows an example of 3D morphology of the surface after the SP process.

The surface topography and its roughness values vary according to the shot velocity which depends on the pressure of air carrying the shots. Figure 20 shows the 3D surface of an aluminium alloy 7075-T651 after shot peening with different air pressures. Before the shot peening, the surface roughness R_a was 0.7 µm. A rougher surface can be seen after the shot peening at a higher air pressure which constitutes an increase in the shot velocity. However, at the lowest air pressure of 1.0 bar, the surface experienced very little erosion while the roughness increased slightly as shown in Fig. 20a. They speculated that the low air pressure cannot effectively push a large shot thus roughening the surface less. A further increase in air pressure causes rougher surfaces as shown in Fig. 20b–f. These similar results were also found by Wu et al. [86] during shot peening of 18CrNiMo steel where the surface developed more pits and protrusions with the increase of shot intensity from a higher air pressure.

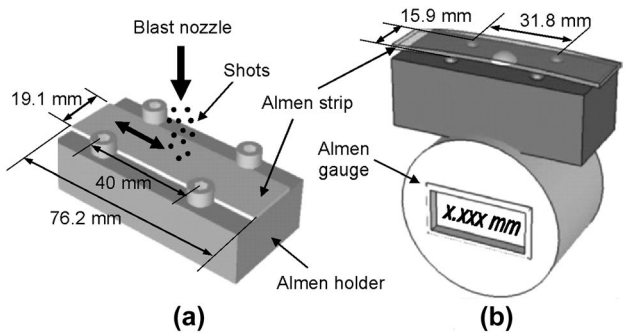

Fig. 18 **a** The Almen strip is peened on an Almen holder, **b** the Almen arc height is measured using the Almen gauge [60]

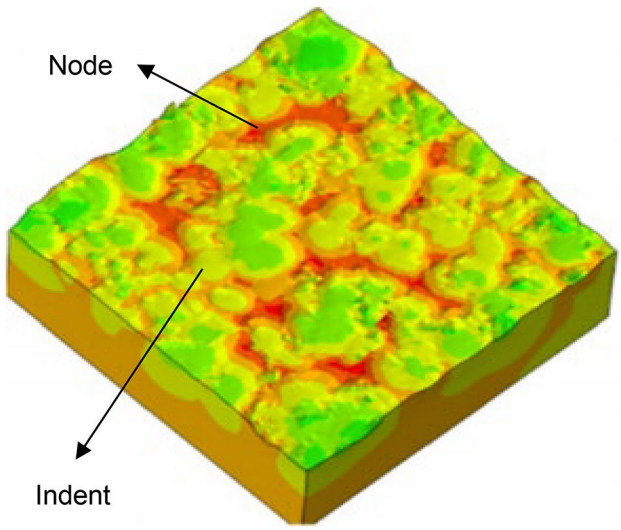

Fig.19 3D Morphology of an Al 7075-T651 surface after to the shot peening [65]

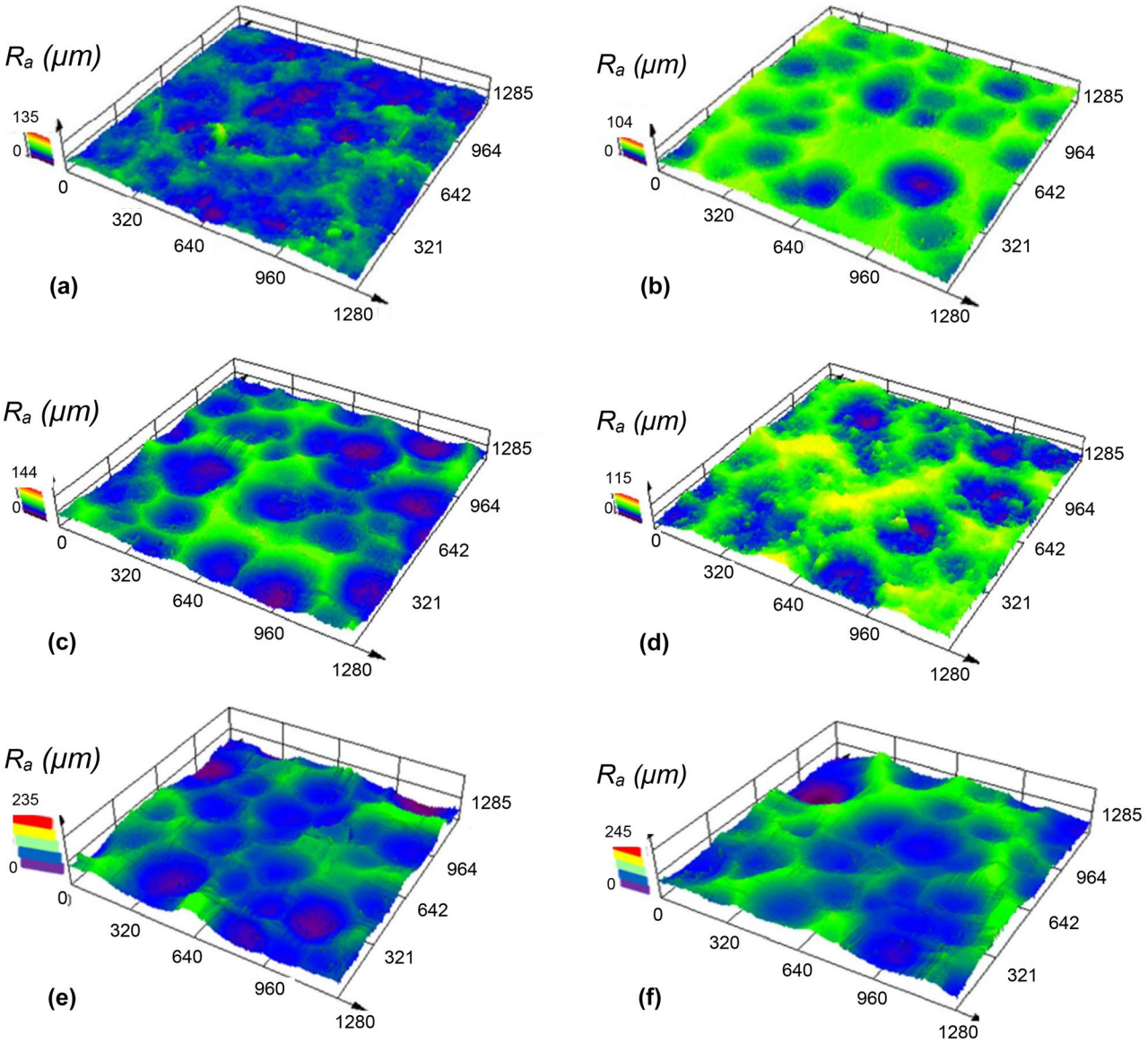

Fig. 20 Roughness after shot peening of Al 7075-T651 at air pressure of **a** 1.0 bar, **b** 1.5 bar, **c** 2.0 bar, **d** 2.5 bar, **e** 3.0 bar and **f** 4.0 bar [65]

An illustration of welded specimens experiencing different levels of shot intensity is shown in Fig. 21. The surface topography changes according to its intensity level for low and high as shown in Fig. 21a and b respectively. The material used was aluminium alloy 6061-T6. Table 2 shows the comparison of their effects after the shot peening process at different intensity levels [20, 68].

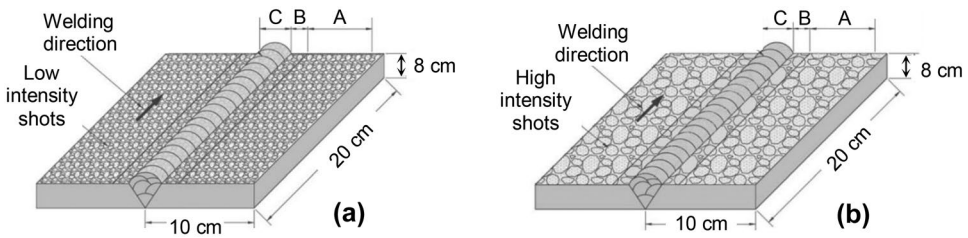

Fig. 21 **a** surface topography of low intensity shot peening Aluminium alloy 6061-T6 [67], and **b** surface topography of high intensity shot peening [67]

Table 2 Comparison on effect of low and high intensity shot peening on aluminium 6061-T6

Material	Shot peening intensity	Alignment	Cracks	Residual stress	Fatigue life
Aluminium **6061-T6**	Low intensity peening	Unstable	Exit	Low	Low
	High intensity peening	Stable	merged	High	High

4.2.2 Effect of shot peening on mechanical properties of metallic surface

The most common effect on mechanical properties for a shot-peened specimen is the introduction of residual stresses over its surface. These residual stresses may be helpful depending on the sign, magnitude and distribution of these stresses [12]. The most popular residual stress classification applies to the coverage region, which may be macroscopic, microscopic or sub microscopic [29]. Surface improvement by peening enhances the fatigue strength and life span through the introduction of compressive residual stresses. An optimization of the SP process can introduce bottomless stresses than the traditional SP thus increasing the lifespan of certain parts by up to 1000% [69]. Also, surface hardening occurs as a residual compressive stress is induced into the surface. Hence, many engineering components have been properly designed using advanced manufacturing methods including surface treatments to produce greater fatigue strength with the introduction of compressive residual stresses on their surfaces. This increase in the fatigue life can be attributed to the compressive residual stresses in the vicinity of the crack tip following the overload cycle [70]. Furthermore, the application of peening processes transforms the high tensile stress into compressive residual stress thus improving the life phase of components and increasing their deformation behaviour [71].

Figure 22 shows images of the surfaces and edges of non-peened and shot-peened specimens to determine its effect on the fatigue strength after shot peening. Using a digital microscope, Fig. 22a was created by stacking images that were viewed at an angle of roughly 45° to the

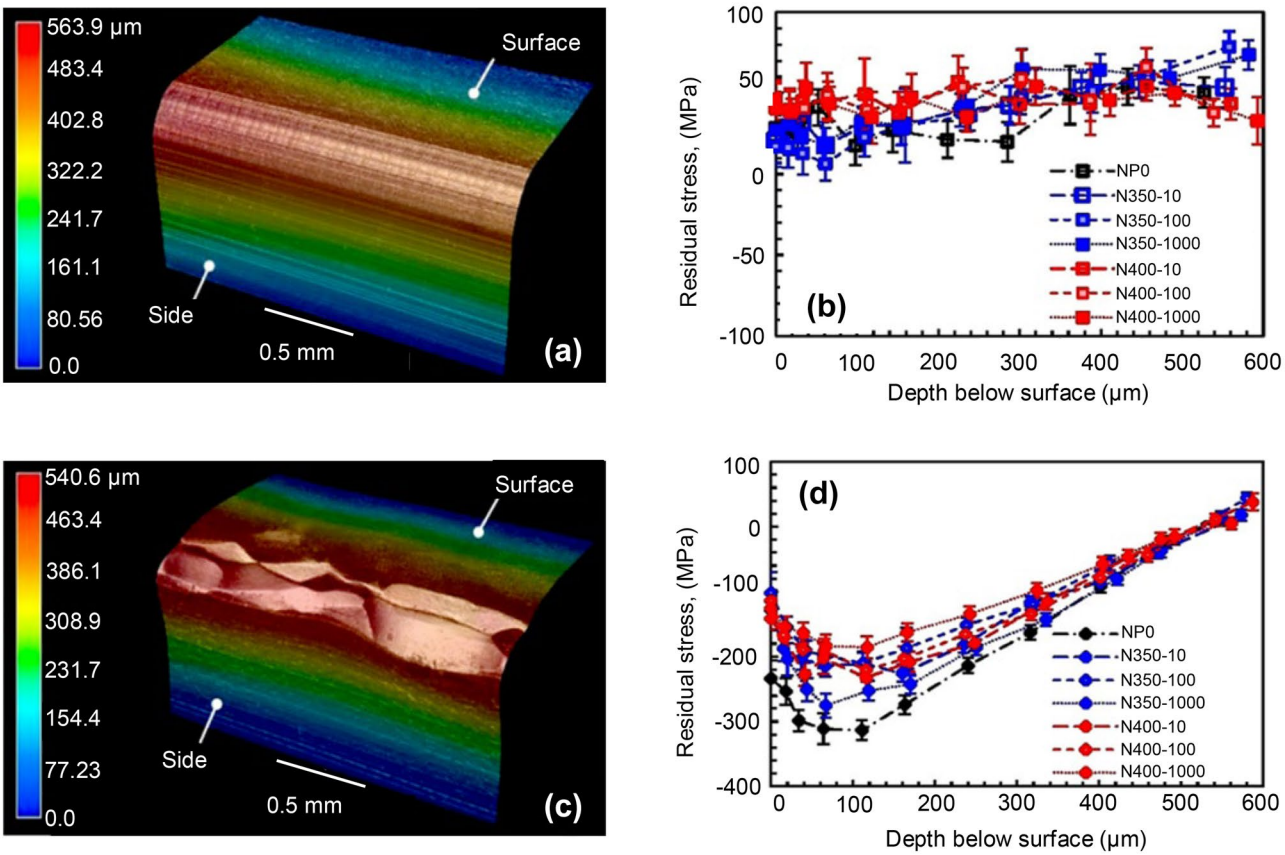

Fig. 22 Aspects of edges of stainless steel SUS316 L specimens and residual stresses as a function of depth below the surface respectively for **a**, **b** unpeened and **d**, **c** shot-peened [72]

surface with a colour map of height along the 45° axis [72]. The edge of the non-peened specimen of stainless steel SUS316 L was rounded with a radius of 0.2 μm using a chamfering tool. Figure 22c shows the surface of the specimen subjected to peening on the upper right-hand side. Shot peening, on the other hand, produces significant edge deformation as compared to non-peened specimens. This plastic deformation would result in fractures with lesser applied stress. Figure 22b and d show the residual stress for non-peened and shot-peened specimens before and after the fatigue test. The 2D X-ray diffraction technique was used to make the measurements. The compressive residual stress was introduced by shot peening. The compressive residual stress decreased after the fatigue test. The reduction in stress was more remarkable when the applied stress was larger and/or the number of cycles was greater. Even for the non-peened specimen, the residual stress became more tensile [66, 73].

Figure 23 shows gradient curves of residual stress along the depth for the non-peening and shot peening cases. As for the non-peening condition, because of heat treatment and grinding, the magnitudes of compressive residual stresses reach the largest on the surface. However, since high velocity shots impact on the surface, a plastic deformation layer with a certain depth is generated. Thus, the maximum magnitude of compressive residual stress shifts to the subsurface. Comparing between the cases of 100% coverage and of 200%, there is no significant difference in the residual stress gradient curve along the depth. The residual compressive stress reaches the maximum of 1150 MPa around the depth of 0.05 mm. After that, it gradually decreases tending to follow the non-peened curve below the depth of around 0.18 mm thus indicating that the affected zone of shot peening reaches 0.18 mm in depth, in regard to the residual stress [74].

Figure 24a shows the surface hardness gradients of the shot-peened Ti-6Al-4 V specimens. The hardness near the surface was stimulated by the shot peening treatment. The maximum hardness value was at least 55 H_V higher than the original hardness around 300 H_V. A strain hardening layer was formed in the surface of the specimen subjected to the SP process. The depth of the strain hardening layer increased from 90 to 135 μm as the SP intensity rose from 0.2 to 0.4 mmA [75]. The micro hardness profiles along the depth of three treatment conditions are shown in Fig. 24b. The surface hardness without peening is around 690 H_V, and the hardness reaches a maximum of 702 H_V at the depth of 200 μm, then it gradually decreases with the distance from surface increases. It is worth noting that as shot peening applies, the surface hardness increases in a visible way. When the shot peening coverage is 100%, the surface hardness increases by 3.3% compared with the non-peened, reaching 712 H_V. When the coverage increases to 200%, the surface hardness continues to increase to 738 H_V, by 6.9% compared to the non-peened case [75]. In addition, when shot peening is applied, the maximum value of hardness appears on the surface. In engineering practice, some empirical hardness equations are recommended, from which the maximum hardness is found to appear at the surface.

4.2.3 Effect of shot peening on microstructural changes of metallic surface

Various parameters in the SP process influence the change of microstructures of the peened specimens. The major factors include the shot intensity, air pressure and exposure time. A method to increase the exposure time is to treat the surface with multiple passes treatment. The effect on microstructures by single and double shot peening is shown Fig. 25. The

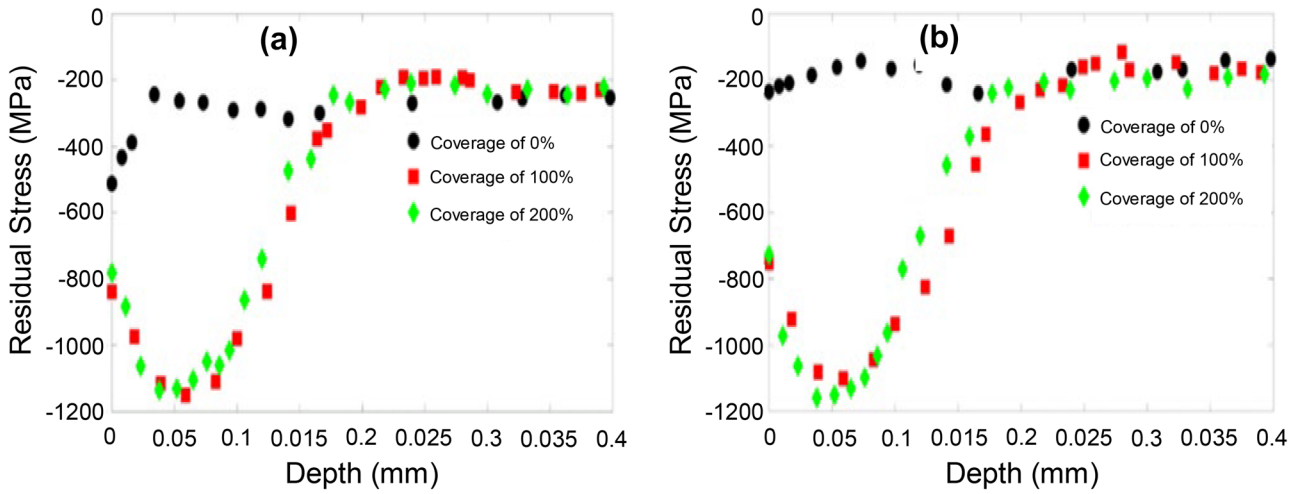

Fig. 23 Gradients of residual compressive stress for carburized 18CrNiMo specimens **a** axial and **b** tangential [74]

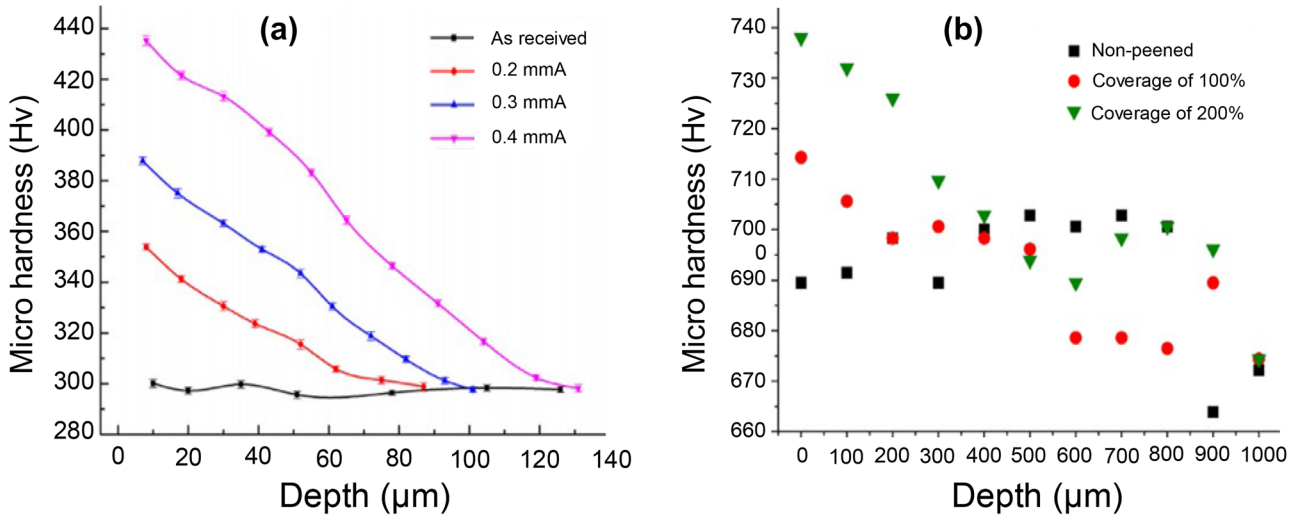

Fig. 24 **a** Surface hardness gradients for the shot-peened Ti-6Al-4 V specimens [75], and **b** micro hardness profile with different shot peening coverage [75]

original specimen without treatment shows a uniform grain size across the cross section as shown in Fig. 25a. After the treatment with both single and double shot peening, it can be found that the grain size at the surface and near-surface develops into slightly finer size as shown in Fig. 25b and c, respectively, within the depth range of 180 μm. However, the depth of the grain refinement zone is almost identical for both single and double SP processes. Furthermore, this grain refinement near-surface is believed to be one of the reasons causing an increase in the surface hardness consequently improving the fatigue resistance of material [74].

Microstructures of metallic surfaces have also been influenced by the shot intensity. Figure 26 shows the scanning electron microscopy (SEM) images of the shot-peened surface at different intensities. It can be observed that typical crater-like marks of repeated shot impacts are clearly seen on all surfaces. Statistically, the surface of sample which belongs to SP30 is significantly smoother than those of specimen SP50 and SP70, from which they concluded that lower peening intensity leads to smaller surface roughness [56]. This may result in an increase in the fatigue cycle of components since the roughness of material plays an important role in the fatigue cycle.

Figure 27 shows the effects of continuous pressure changes in the SP process on the material surface. The original specimen shows a grainy structure as seen in Fig. 27a and b. In general, shot-peened specimens display rough surfaces and voids in the deformed layer as shown in Fig. 27c–d. As the air pressure increases to 482.6 kPa, the microstructure shows the columnar features with a deeper

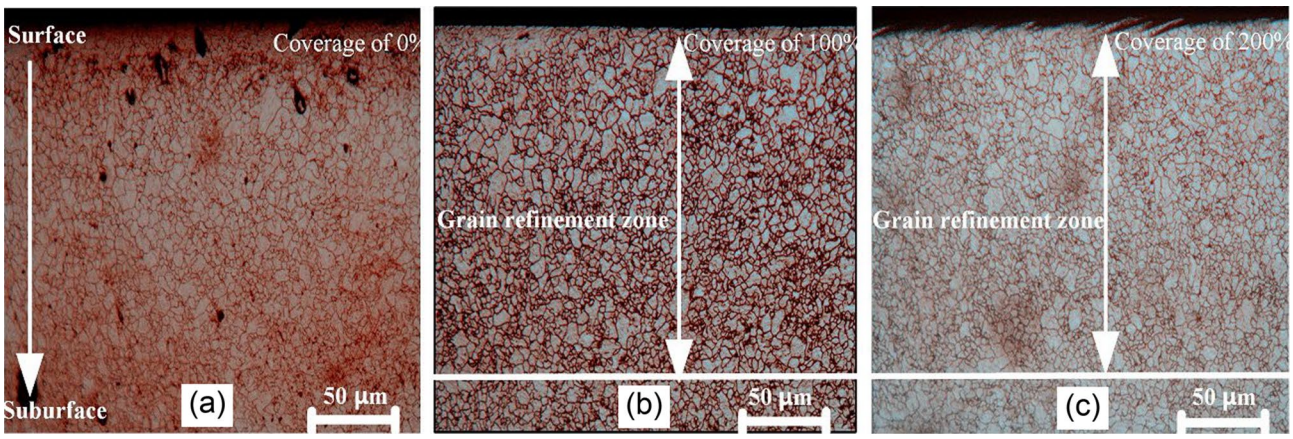

Fig. 25 Comparison of grain size for carburized 18CrNiMo specimens with **a** no treatment, **b** single treatment (100% coverage) and **c** double treatment (200% coverage) [74]

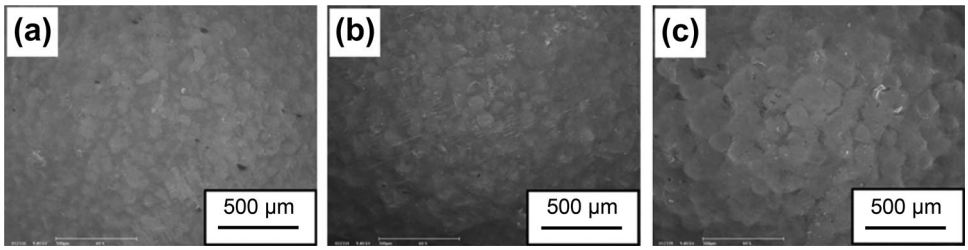

Fig. 26 Images for Ti-6Al-4 V specimens under different shot peening **a** SP 30 **b** SP 50 **c** SP 70 [76]

grainy layer as shown in Fig. 27e and f. This may essentially prevent the growth of fatigue cracks. However, at the highest air pressure of 689.5 kPa, the surface experiences more damage with large dents and possible stress concentration as shown in Fig. 27g and h. This will lead to a higher amount of fatigue initiations sites thus reducing the fatigue performance of material. This shows that the SP process can produce a deformed layer with columnar features thus improving the fatigue life of a material; however, an excessive air pressure may cause more damage to the surface [76].

Figure 28 shows the microstructural changes of shot-peened specimens with different air pressures but same duration of peening time. The images were initially taken using scanning electron microscope as shown on the left side. Then, the SEM images were modified into a binary image as shown on the right side to evaluate the faulty region as indicated in red colour in which the background was converted to white and the percentage of micro cracks and the area of defects relative to the area of the whole image were calculated using an image processing technique. The microstructure of the original specimen is shown in Fig. 28a and b. The dislocation clusters and micro-cracks were reduced after SP at an air pressure of 206.8 kPa as shown in Fig. 28c and d. When the air pressure increases to 482.6 kPa, the microstructure improves significantly as shown in Fig. 28e and f with the smallest area of defects. However, the surface deteriorated at the highest air pressure of 689.6 kPa as shown in Fig. 28g and h with large defects.

Tables 3 and 4 compare the effects of two different materials, namely carbon nanotube/Al–Mg-Si and Al–Mg-Si alloy after the SP process. It can be noted that the roughness is about 15% higher in the case of the composite material possibly due to their microstructure with irregular structure as shown in Table 3. Table 4 shows that the hardness is higher in composite material due to invocation of compression and relaxation of material after the shot peening [76].

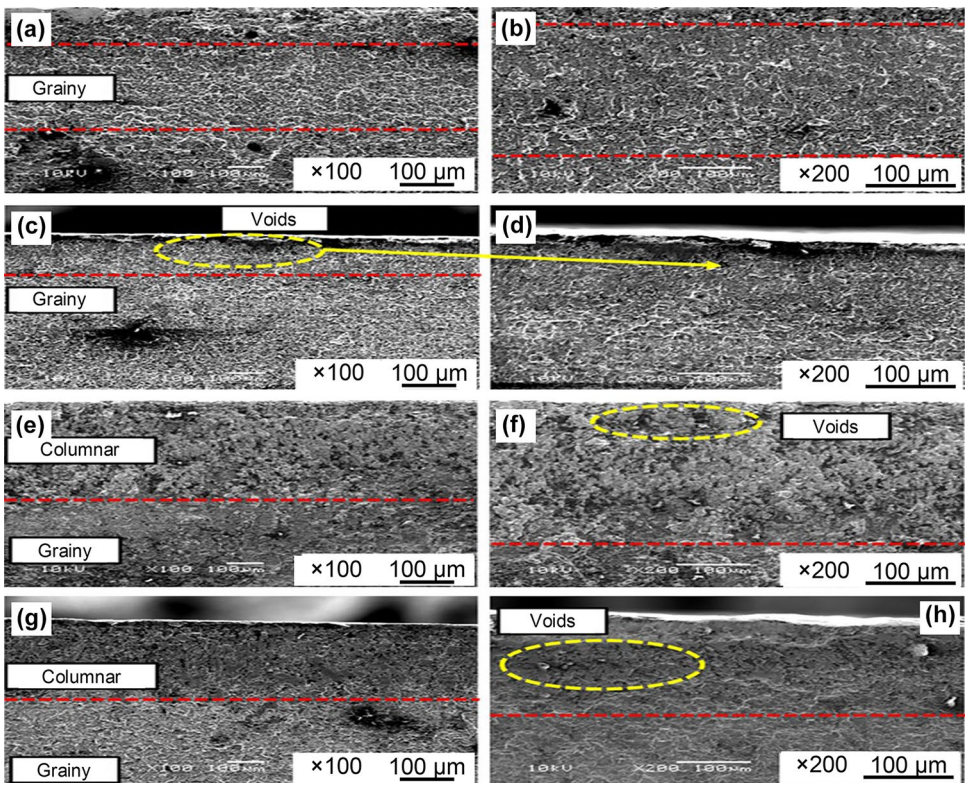

Fig. 27 Fractographic images for Ti-6Al-4 V specimens **a**, **b** intrinsic; **c**, **d** SP30; **e**, **f** SP50; **g**, **h** SP70. The yellow-dotted circle denotes the gap located zone, while the red-dotted line denotes the boundary between various layers [76]

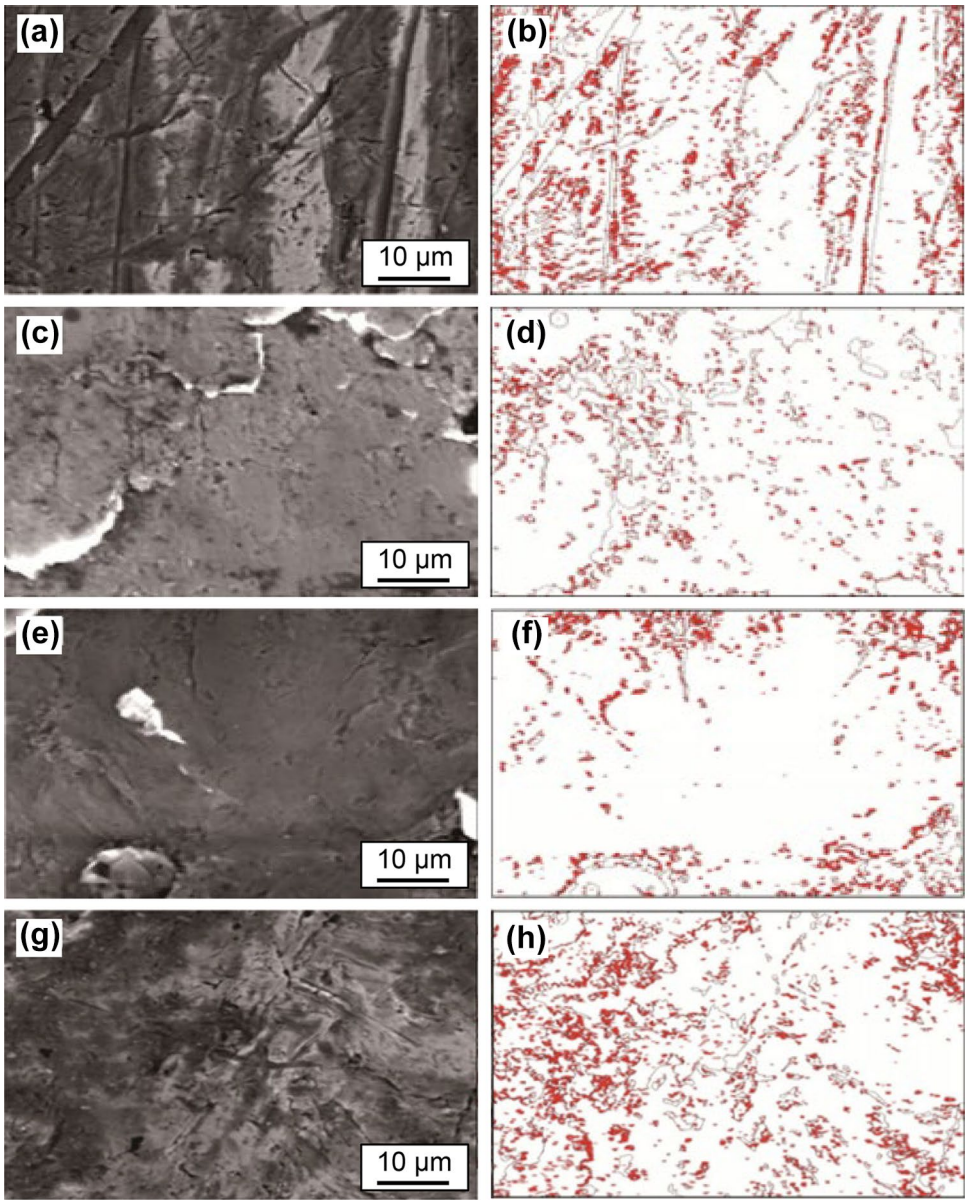

Fig. 28 Microstructure for steel 1070 specimens with different air pressures **a b** original, **c d** 206.8 kPa, **e f** 482.6 kPa, **g h** 689.6 kPa [21]

In conclusion, Table 5 has summarised all responses on surfaces and sub-surfaces for various studies in the SP process. The studies involve different types of materials and processing parameters. There are more opportunities for future research in the SP process for new metallic materials in specific industrial applications.

Table 3 Comparison on roughness effect of composite and Al–Mg-Si alloy

Ref	*Materials*	R_a *(μm)*	R_z *(μm)*
[3, 60]	Carbon nanotube (CNT)/ Al–Mg–Si composite	65	67
[4]	Al–Mg–Si alloy	55	59

5 Laser shock peening

In surface treatment technology, laser shock peening (LSP) has been known to be an advanced and innovative technique that improves the surface properties. The process can effectively boost fatigue life and strength with mechanical

Table 4 Comparison on effect of hardness and residual stress of composite and Al–Mg-Si alloy

Ref	*Materials*	*Hardness* (H_V)	*Residual Stress (MPa)*
[1, 3, 5]	CNT/ Al–Mg–Si composite	106	97
[4]	Al–Mg–Si alloy	93	133

Table 5 Summary of responses on surfaces and sub-surfaces for various studies in SP process

Ref	Materials	Parameters	Responses
[80]	Aluminium Alloy	Shot velocity (32–72 m/s), angle 90°, shot size (1.16 mm), SOD (150 mm)	Stress changes in positive
[57]	Carburized stainless steel	Intensity (12–16 A), shot diameter (0.4 and 0.6 mm), coverage 100%	Residual stress decreases
[76]	Titanium alloy	Pressure (30–70 psi), intensity (6–11 A), shot flow rate (10 lb/min),	Roughness on surface
[81, 82]	41CrAlMo7 steel	Tungsten carbide (0.65 and 0.9 mm), air pressure (4 bar), SOD (400–420 mm), exposure time (15 and 18 min),	Quenching, tempering, nitriding, and double SP are increased in residual stress
[69]	AISI Mild Steel	Pressure (4, 5,6 bar), time (60, 90, 120 s), SOD (50, 100,150 mm)	Pressure and time increase in tensile strength
[62, 77]	CNT/6061 Al composite	Nozzle diameter (15 mm), SOD (100 mm), time (0.5 min), shot diameter (0.25 and 0.42 mm), pressure (0.08, 0.12, 0.15, 0.20, 0.30 MPa), intensity (0.05, 0.1, 0.15, 0.20, 0.25 A)	Surface roughness increases. Corrosion reduction and fatigue growth rate increase with surface roughness
[83]	Fibre metal laminates (aluminium–lithium alloy)	Ceramics shots (0.4 mm), time (1 to 9 s), coverage 100%, intensity (0.09 to 0.19 A)	Fibre layers significantly affected the deformation behaviour
[84]	CNTs)-reinforced Al–Mg–Si composite	Intensity (9 A), ceramics shots (0.3 mm), annealing temp (150, 200, 250 °C)	CRS (compressive residual stress) decreases when annealing temperature rises
[85]	ZrB2–SiC composites	Zirconium oxide shot (0.3 mm), pressure (0.1 to 0.4 MPa), time 20 s	Fatigue strength depends upon the pressure
[86]	18CrNiMo7-6 steel	Cast steel shots (0.28 and 0.58 mm), pressure (0.1 to 0.5 MPa), angle (90^0), distance (180 to 220 mm), coverage 200%, flow rate (4 to 12 kg/min), nozzle diameter (4 mm)	Residual stress increase and surface roughness has a direct link with hardness
[87]	39NiCrMo3 low alloy steel	AGB 70 shots (0.7 mm), intensity (13 A), time (7 s), coverage 100%, tempered (600 °C at 2 h)	Hardness increases with improvements in roughness
[88]	AA2024-T3 alloy	Pressure (0.5 MPa), distance (60 mm), nickel shots,	Increased fatigue and flexural stress
[89]	(TiB + TiC)/Ti-6Al-4 V titanium matrix composite	Intensity (0.1 mmA), nozzle diameter (8 mm), ceramics shot diameter (0.30 mm), coverage 200%,	Improved CRS and hardness
[90]	Aluminium borate ($Al_{18}B_4O_{33}$) reinforced Al–Mg-Si composite	Ceramic + glass shot diameter (0.35 + 0.045) mm, intensities (0.25, 0.40, 0.45 + 0.08) mmN, time (20 + 10) s	Dislocation density, roughness and corrosion increase
[78]	2124-T4 aluminium alloy silicon carbide composite	Steel shot diameter (0.8 mm), time (10 s), pressure (0.3 MPa),	Hardness and residual stress increase with particle density high

properties of components by applying the compressive stress with a laser shock wave and improve cracks of the metallic components [91, 92]. For surface treatment, a high-energy pulsed laser beam strikes the metal component, creating high-amplitude stress waves [93]. In comparison to other traditional surface treatments, LSP offers three distinct benefits: a controllable heat source, low heat distortion and high structural adaptability [94].

The surface material resists the tension waves, extending and causing the creation of a surface compression stress [95]. LSP is used to reduce the susceptibility of stainless steel and other metallic materials to surface corrosion cracking (SCC) by removing the impulsive force of high-pressure plasma. By developing a nanostructured surface with an average depth of less than 10 µm, LSP improved ultimate tensile strength and elongation rate [96].

5.1 Working principle of laser shock peening

As shown in Fig. 29, to prepare a component for laser peening, apply an overlay to the material surface to be handled that is opaque to the laser beam. The paint (dry or

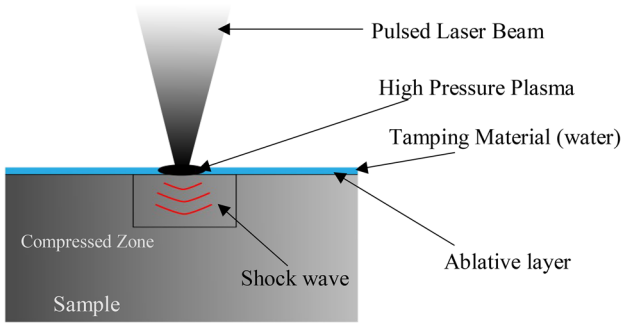

Fig. 29 Schematic view of laser shock peening process

wet), black tape and metal foils (with or without adhesive backing) have all been used as opaque overlays, with varying but similar results in terms of pressure pulses produced [97]. The dark overlay prevents the surface from overt warm contact with the laser-incited plasma and creates a consistent surface for laser beam interaction, releasing the original substance being processed [98]. Depending on the laser irradiation conditions and metal properties, direct interaction of a metal surface with plasma can result in the creation of a thin melt layer on the metal's surface, ranging from surface discoloration to a surface melt layer 15 to 25 mm thick [99]. The opaque overlay is then covered with a material that is transparent to the laser beam. Water flowing over the surface from an appropriately positioned nozzle, as shown in Fig. 29, is the easiest and most cost-effective transparent overlay [100]. The water does not cool the component, but it does play an important role in restricting the plasma produced in the meantime the laser beam is going to relate with the opaque overlay surface [79, 101]. The laser beam passes through the water and interacts with the transparent overlay. Then the laser energy is absorbed by the invisible overlay layer in the first few micrometres, allowing the material to vaporise and plasma to form [102, 103]. The temperature of the plasma rapidly rises due to additional heating by the incoming laser beam, but its thermal expansion is constrained by the transparent overlay material [104].

Laser shock peening process is influenced by several parameters and factors. The typical parameters and their levels are illustrated in Fig. 30 [92, 105]. The typical parameters include duration of the pulse, diameter of the laser spot and focal spot size.

Figure 31 shows the laser shock peening spot position and the percent of the overlapping ratio of spots. The laser impact must be optimised by controlling the direction of spot and ratio of overlapping and also the direction of scanning is a key factor in laser shock peening [114].

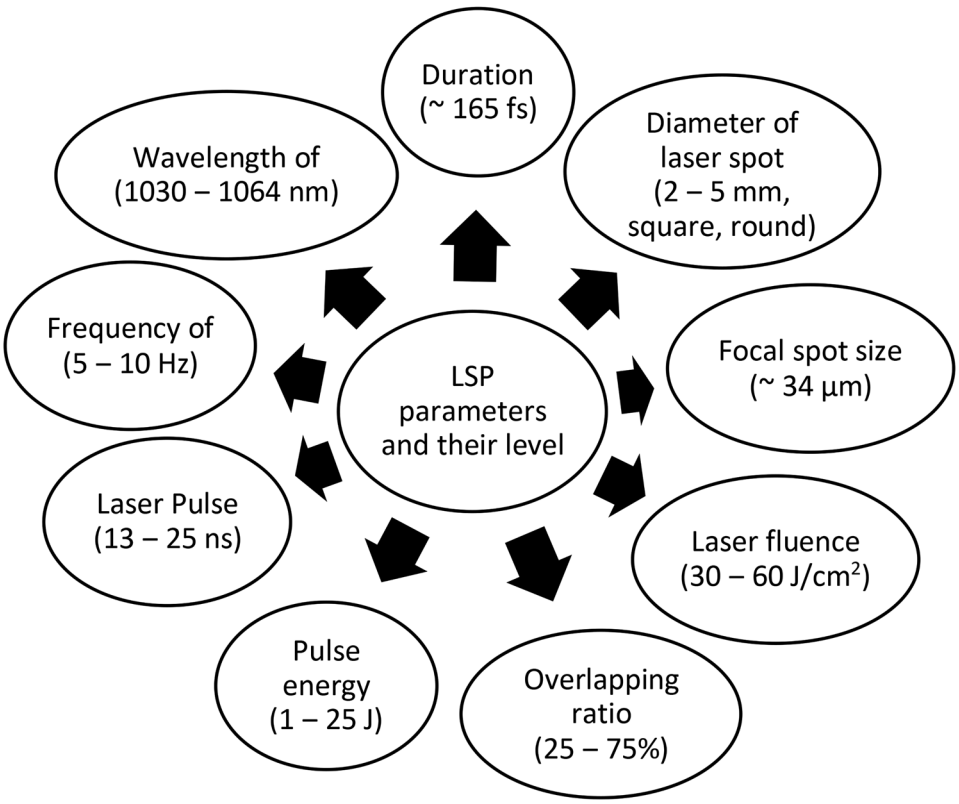

Fig. 30 Typical laser shock peening parameters and their levels

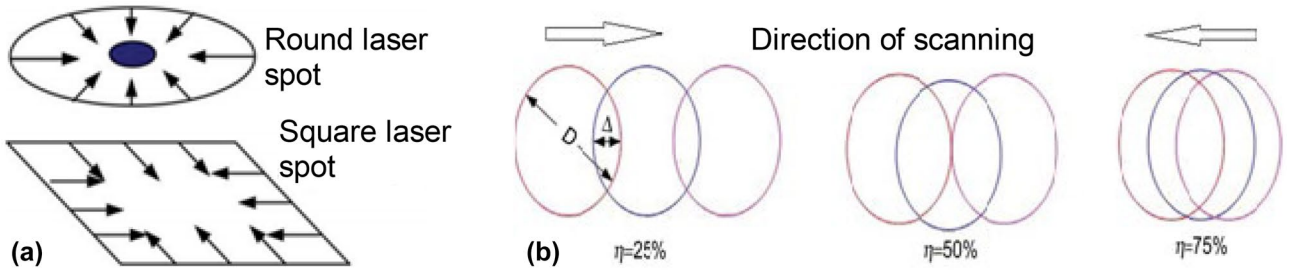

Fig. 31 Schematic views of LSP **a** laser spots **b** laser spots over lapping

5.2 Effect of laser shock peening on metallic surfaces

The effect of laser shock peening on metallic surfaces is interestingly getting attention as the improvement on the mechanical and microstructural properties has practically been realised. The mechanical and microstructural changes have been studied using several techniques such as tensile testing, surface roughness, residual stress analysis, Vickers micro hardness and X-ray diffraction. Li et al. [96] used three types of LSP specimens and were analysed for tensile strength, elongation intensity, and detailed microstructural evolutions and the mechanisms of surface nanocrystallization and amorphization. Residual stress increases by a change in laser impact around 414.8 to 448 MPa; however, continuous increase reveals the effect of stresses to be negative [94].

In LSP, a pressure is applied on the surface of the materials in nanoseconds and a local plastic deformation is developed. The pressure applied is beyond the dynamic yield strength of the materials and this leads to a residual stress that improves the mechanical properties of the localised part of the material. In light of this, several works of finite element analysis have been done to predict the residual stress due to the SLP [106–108].

Ding et al. [108] predicted the distribution of residual stress based on the dislocation density-based material model which indicates that the magnitude and the profile show similarity within the material depth of 0.7 mm. Figure 32 shows the predicted and the experimental results of the distribution of the residual stress in aluminium (LY2) materials where the impacts were 5 times and positioned in the horizontal direction. Similarly, Xiang et al. [107] in their numerical simulation of LSP, it was predicted and reported that the shape of the spots did not have an effect on the performance of the residual stress distribution; however, the scanning pattern profile would create significant effect on the surface quality and residual stress distribution.

Besides the overall operation and interaction between the shockwave and the metallic parts, the understanding of the

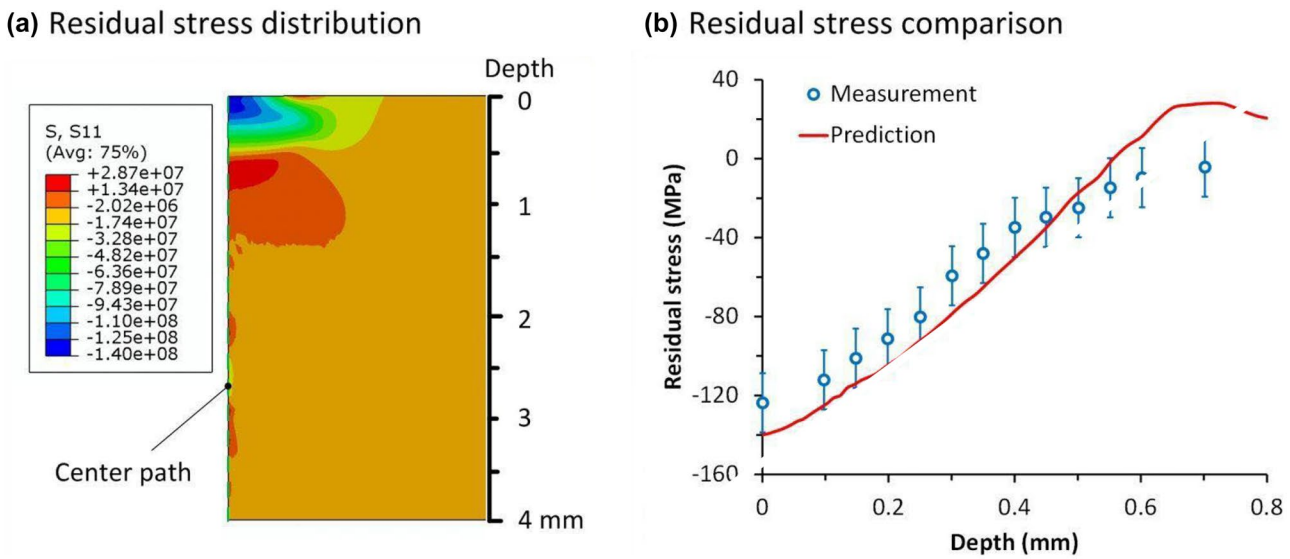

Fig. 32 Experimental vs numerical analysis results of residual stress for LY2 aluminium alloy [108]. **a** Residual stress distribution, **b** residual stress comparison

quantity of pressure of shock wave applied on the metallic surface is very important. Several researchers [106, 109, 110] in determining the shock wave pressure over a specified time on the metallic surface estimated that the peak pressure can be calculated as Eq. (1) [107, 111].

$$P_{peak}(GPA) = 0.01 \times \sqrt{\alpha/(2\alpha+3)} \times \sqrt{Z(g.cm^{-2}.s^{-1}} \times \sqrt{I_0(GW.cm^{-2}} \quad (1)$$

where α (0.1–0.2) represents the efficiency of the interaction, Z is the acoustic impedance of the target and constraint layer to the shock wave and I_o is the power density which is defined as Eq. 2.

$$I_o = \frac{4\gamma E}{(\tau.\pi R^2)} \quad (2)$$

where γ is the absorption coefficient (0.8–0.95), E is the laser energy (J), τ is the laser pulse width and R is the spot diameter. The shock wave acoustic impedance (Z) between the target and constraint layer is defined as Eq. (3).

$$\frac{2}{Z} = \frac{1}{Z_{target}} + \frac{1}{Z_{confine}} \quad (3)$$

where Z_{target} and $Z_{confine}$ are acoustic impedance of the target and constrained layer material respectively.

Based on the Hugoniot elastic limit (HEL), the induced shock wave is practically set 2–3 times the material's property of the peak pressure (P_{peak}) and the persisting action time was also 2–3 times the laser pulse duration which gives better effect on the performance of the shot peening [112].

5.2.1 Effect of laser shock peening on topography of metallic surface

The LSP has a roughness increase resulting as compared to SP. The SP method has a negative effect since it usually increases the surface roughness, which increases crack nucleation [113]. This effect is much more harmful because the surface roughness before SP is smooth and the substrate is notch-sensitive [113]. Through numerous progressive and regulated impacts of pulsed laser beams, the LSP technique may generate high-intensity shock waves that then cause hundreds MPa of compressive residual stress [114].

Gao et al. [115] investigated the effect of pulse energy on the surface roughness of nickel aluminium bronze alloy (NAB) materials and showed that the surface roughness (R_a) has increased rapidly as the laser pulse energy progressively increases. The untreated NAB specimen R_a had a surface roughness of 4.85 µm. According to the experiment, the R_a values were 3.27 µm, 4.11 µm and 6.17 µm for the laser pulse energy applied was 2 J, 4 J and 6 J, respectively. Figure 33 revealed the values of the surface roughness on different energy pulses. On the other hand, the compressive stress developed by the application of LSP on AZ31B Mg alloy had limited the stress corrosion cracking (SCC) initiation and development on the surface [115].

5.2.2 Effect of laser shock peening on mechanical properties of metallic surface

The application of laser shot peening on steel materials is commonly known for its improvement in the mechanical properties of materials on the surface. The effect of the LSP on the hardness, ultimate tensile strength and fatigue life of metallic materials has been studied thoroughly. For example, Lu et al. [116] used H62 brass material to study the effect of LSP on the ultimate strength and elongation rate and found that both properties were improved when treated for less than 10 nm depth. However, Yong et al. [117] use 32CrNi alloy steel and found that the ultimate strength had no change in value before and after the LSP whereas yield strength and elongation decreases. At the same time, micro hardness and fatigue life have been improved. It also discovered that ultra-high strain rates were more likely to activate dislocation density at a higher temperature, resulting in the disappearance of cracks in the commercially pure titanium plastic deformation layer [118]. Maximum CRS is 750 MPa on optimum temperature. Temperature increases continuously and stress will decrease [115].

According to Fig. 34a, considering the initial residual stress sampling point at a depth of 0.025 mm, surface residual stresses of 55.8 MPa, 57.5 MPa, 82.4 MPa and 95.3 MPa were developed corresponding to laser pulse energies of 0 J (untreated), 2 J, 4 J and 6 J, respectively [115]. In Fig. 34b, the change in micro hardness as the depth of direction indicates that the highest pulse energy resulted in highest micro hardness. Specifically, the highest values of laser pulse energy of 2 J, 4 J and 6 J resulted in 195 H_V, 223 H_V and 241 H_V, respectively. The percent of micro hardness value increase follows as 14.7%, 31.2% and 41.7%, respectively, as compared to the untreated samples [115]. It is also reported that improvement in the fatigue life after the LSP treatment by the proof of fracture morphology and surface micro hardness was 301 H_V, which has increased from the original one but fatigue life has increased by 76% from LSP [119]. It has been investigated that the impact of laser shock peening on the tensile properties, residual tension and microstructure on 2319 aluminium that the high density of dislocations and the mechanical effect caused by LSP resulted in a microhardness increase [96].

Gao et al. [115], in their experiment as shown in Fig. 35, demonstrated that LSP-treated materials registered less initial axial deformation than the untreated. The untreated material's initial axial deformation was 0.348 mm while the

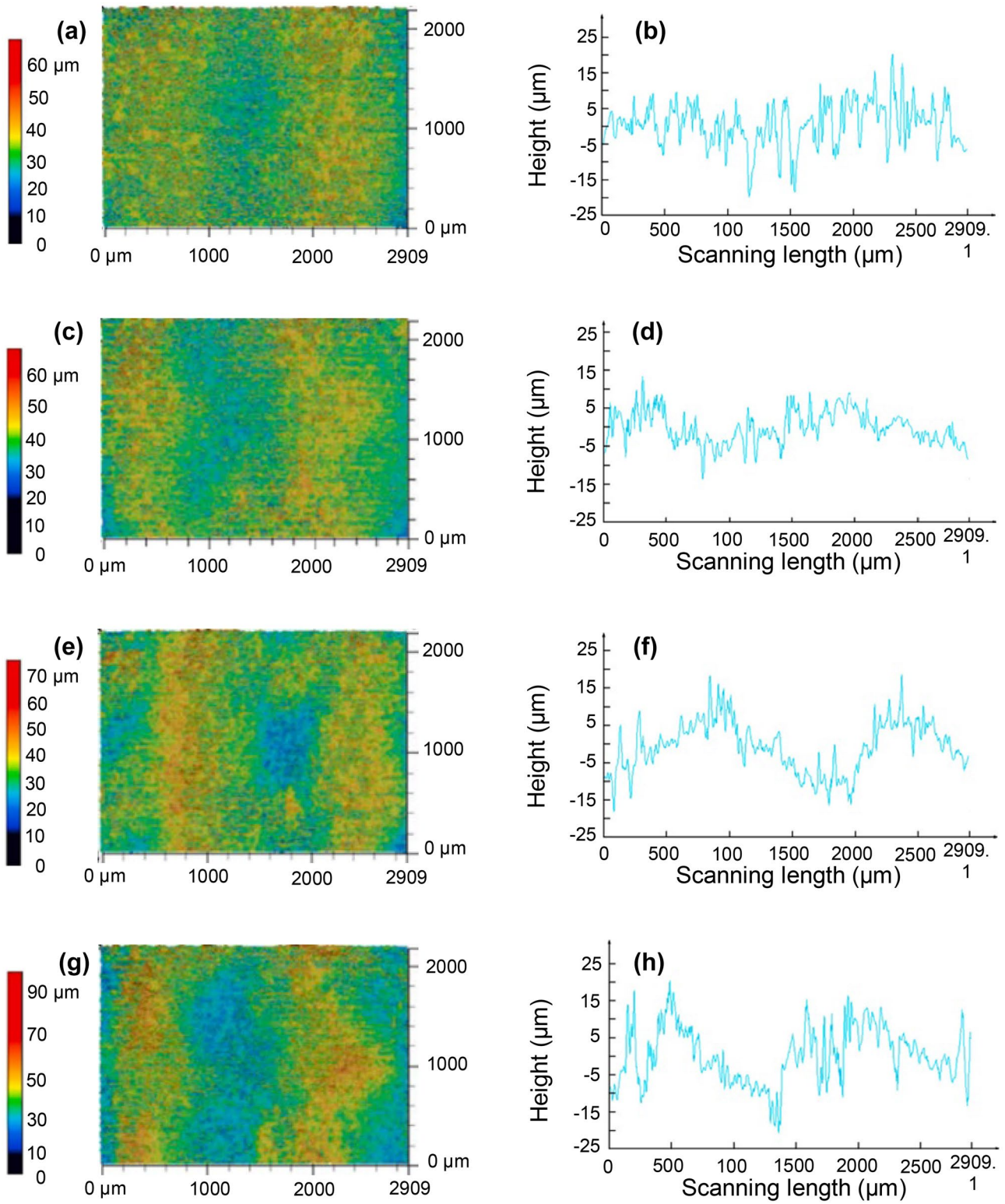

Fig. 33 3D surface topography distribution image for NAB alloy specimens and section roughness profile, respectively, for **a**, **b** unpeened specimen, **c**, **d** energy 2 J specimen, **e**, **f** energy 4 J specimen and **g** and **h** energy 6 J specimen [115]

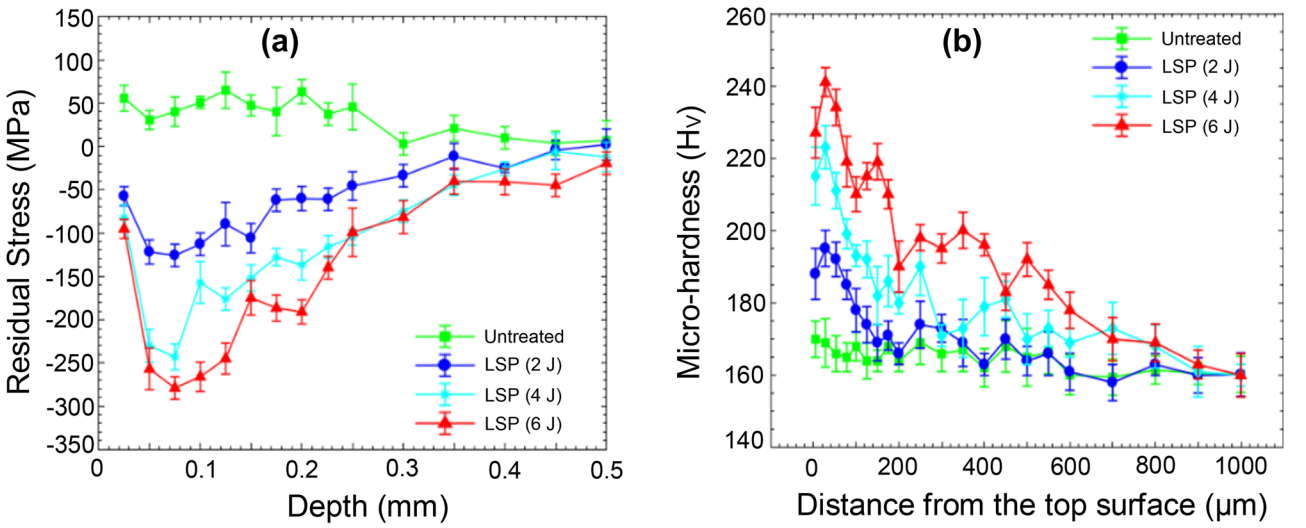

Fig. 34 **a** residual stress distribution of NAB alloy specimens subjected to different laser pulse energies along the depth from the treated surface [115], and **b** micro hardness profiling of treated specimens along the depth [115]

specimens treated with laser pulse energy of 2 J, 4 J and 6 J deformed to 0.347 mm, 0.277 mm and 0.247 mm, respectively. It is also shown in Fig. 35a and b that the trend in both minimum and maximum axial deformation as the fatigue cycles is the same [115]. On the other hand, the surface hardness decreases in the absence of a restricting substrate with a protecting coating [120]. Air consistency after LSP in the air short of coating is superior to that of the untreated surface [121]. Additionally, LSP caused changes in the tensile and compressive stress which actually was residual stresses of the material, resulting in significantly increased yield power [122].

5.2.3 Effect of laser shock peening on microstructural changes of metallic surface

Tensile properties of metallic materials are thought to often result from micro-plastic deformation with change in residual stress [123]. Similarly, Huang et al. [92] investigated the effect of laser peening on tensile properties and microstructural reaction on 2024-T351 aluminium alloy specimens. A higher density of dislocations and smaller-size grain induced by laser peening was responsible for the high strength, plasticity and magnificent tensile properties.

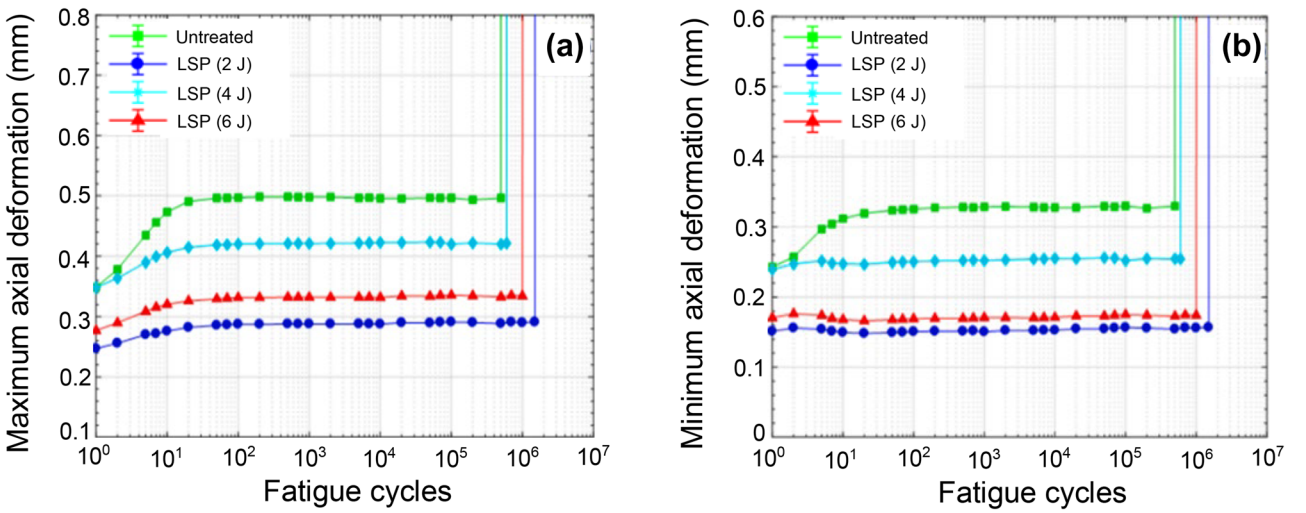

Fig. 35 The experimental curves of axial deformation versus fatigue cycles on NAB alloy specimens subjected to LSP with different laser pulse energies **a** maximum and **b** minimum axial deformation [115]

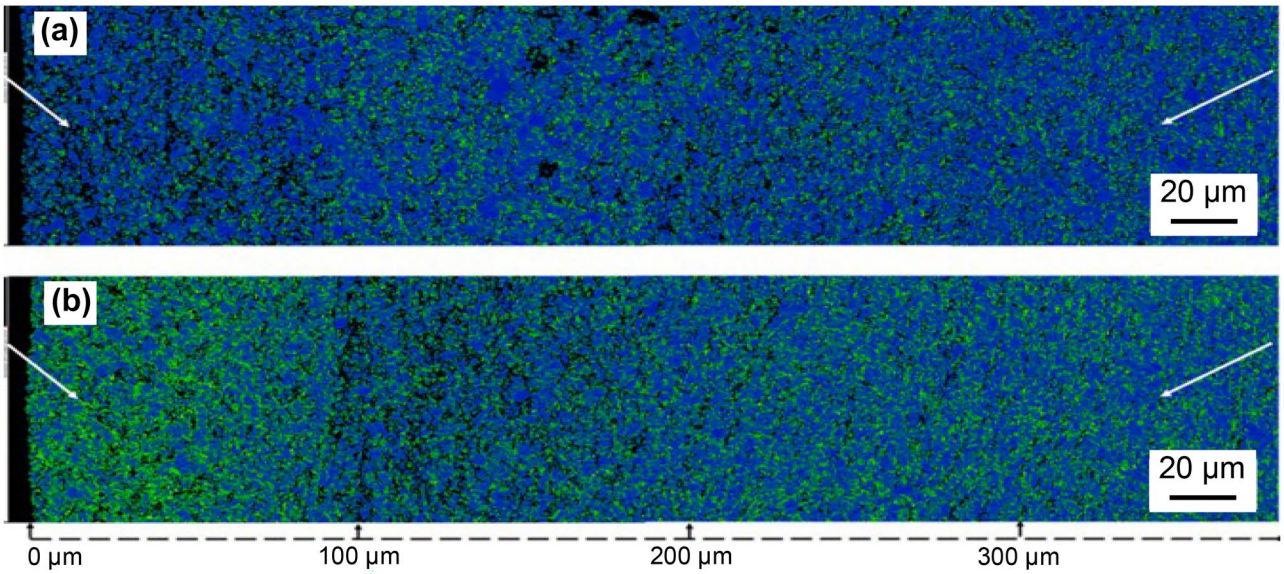

Fig. 36 Morphology structures of different laser peening for Ti6Al4V specimens **a** laser shock peening and **b** warm laser shock peening [127]

The LSP treatment induced the plastic deformation, which is concluded in an excessive increase in dislocation density, resulting in dislocation tangle formation [38, 124]. FEM results have proved that a high number of peening impacts increase the magnitude and depth of CRS [113]. The effect of LSP at unlike process temperatures on the mechanical properties like as microstructural evolution and would be affected tensile of CP titanium which has investigated, and the results revealed that higher process temperatures were associated with greater elongation and area reduction of the laser shock–peened specimens [125].

Figure 36 shows the morphology of laser peening and the boundaries of layer impact after the treatment. It is also showing grain boundary maps in some areas (low-angle boundaries in 200 to 300 μm, high-angle boundaries in 100 to 200 μm) [126]. As compared with the process effect between laser shock peening and warm laser shock peening, the boundaries must be better aligned by warm laser shock peening [113].

Figure 37 shows an example of TEM image of laser peening treatment material showing nanocrystalline structures of the treated surface. The grains are approximately between 30 and 60 nm in size and the nanograin layer is around 100 to 150 nm thick. Region [I] shows a pattern with a panel depth of less than 500 nm. The region marked [II] in the column, at a depth of about 500 nm, was very normal. The LSP sample's grain size formed a gradient distribution along the depth direction, with nanograins at the surface, processed grains in the subsurface and the matrix's original coarse grain in deeper layers [127].

Figure 38a and b at a depth of 15 μm, there is an extreme plastic deformation layer that leads to refined grain, and at a depth of 15–25 μm, there is a transition layer (I) of plastic deformation. However, under the depth of 25 μm, except for flat grains parallel to the surface in the transition layer (II), grain refining is difficult to see [128]. Dislocation motion is triggered during the process. Dislocation movement modes include tangle, recombination, and annihilation.

In the LSP process, the laser shock waves induce substantial plastic deformation on the surface, resulting in higher pile-ups with pits and overlap marks, as seen in Fig. 39c. In comparison to the baseline specimens shown in Fig. 39a, the surface of the LSP-peened specimens has sharp amplitude and a lower valley. In Fig. 39c, there is also noticeable pits and overlap marks. Figure 39d on the surface of the LSP-peened specimens, as seen in surface morphology cloud diagrams, resulting from surface roughness of the LSP peened specimens on the surface improving significantly as compared to baseline specimens. The laser spot's irregular energy distribution on the surface causes homogeneous plastic deformation (pits) [128].

Tables 6 and 7 show the comparisons for the effects of laser shock peening treatment on the roughness and mechanical properties of 304 stainless steel and nickel aluminium bronze alloy (NAB) respectively. From Table 6, it can be observed that roughness has a higher value in the case of NAB alloy than stainless steel [119, 125]. The irregular structure and grain presence in the steel, laser shock peening become the result in the surface roughness differ. The result might be due to the development of irregular structure and coarse grain in the NAB by the laser shock peening [95]. Table 7 also indicates that 304 stainless steel shows higher hardness compared to NAB alloy. However, NAB alloy generates higher residual stress which might be due

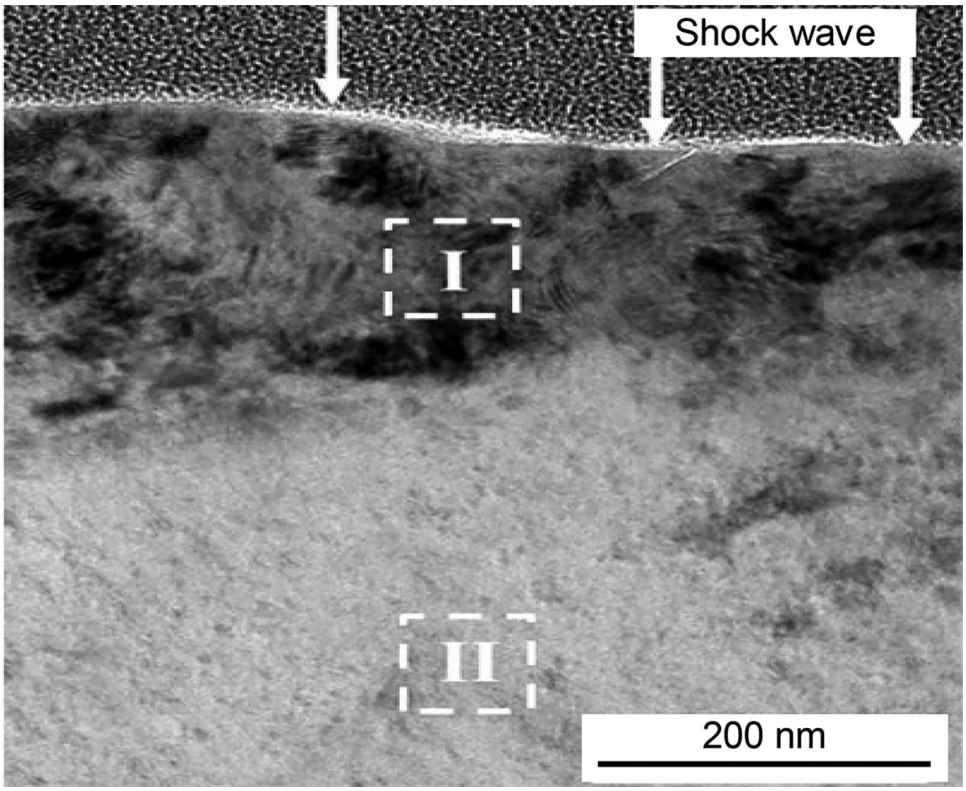

Fig. 37 Cross-sectional TEM image of Ti6Al4V titanium alloy after LSP [127]

to invocation of compression and relaxation of the material after the laser shock peening [95]. Both alloys exhibit lower hardness after the laser shot peening.

In conclusion, the effects of LSP treatment and the relation with each other on surfaces and sub-surfaces are summarised in Table 8.

6 Water jet peening

Another cold mechanical surface treatment process is water jet peening (WJP). Water jet peening is utilised to produce compressive stresses on the surface. This process is considered one of the methods for surface strengthening

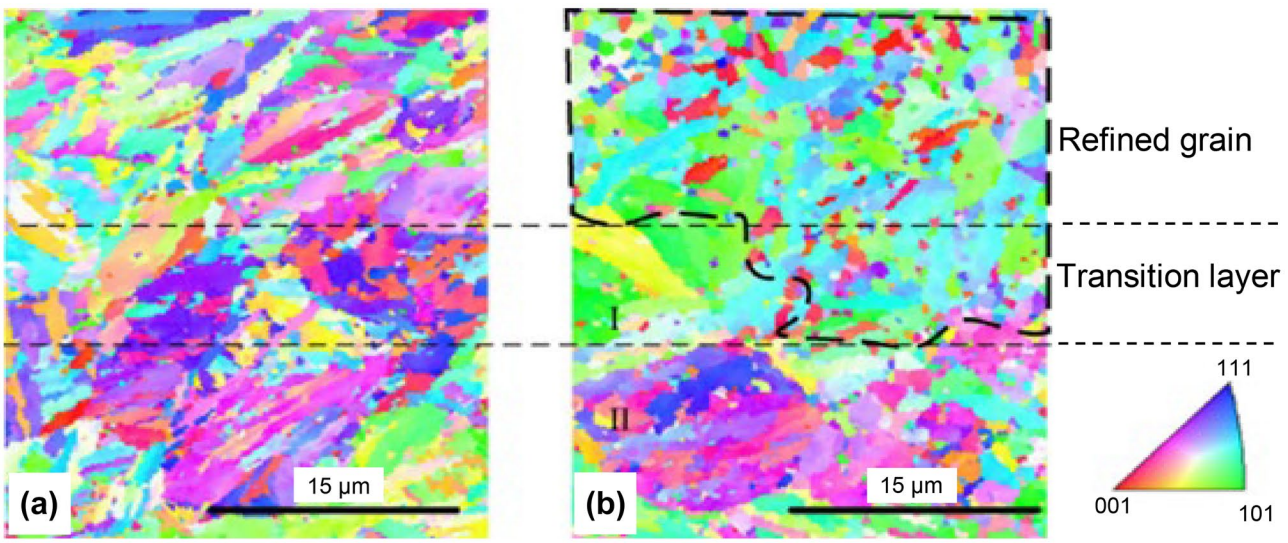

Fig. 38 Electron based inverse pole figure for 32CrNi alloy steel specimens **a** IPF before laser treatment **b** IPF after laser treatment **c** IPF region view [128]

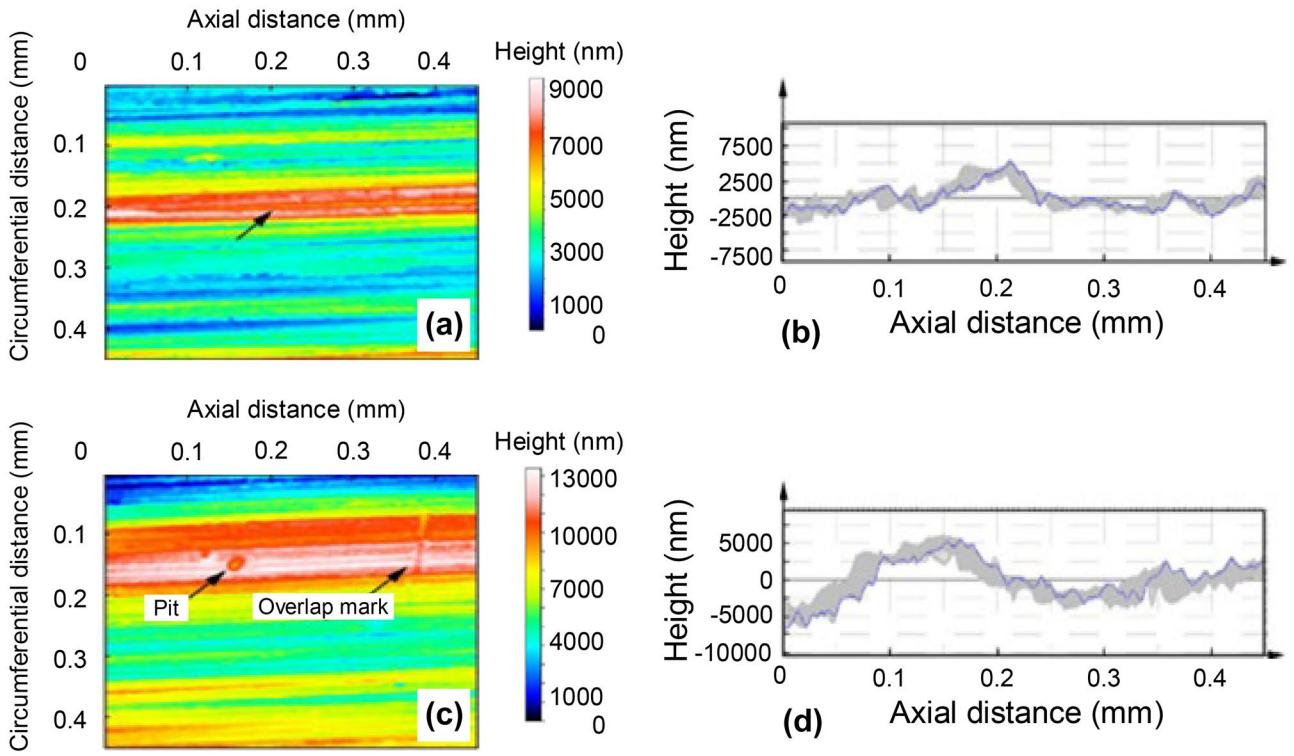

Fig. 39 Surface topography before and after laser shock peening for 32CrNi alloy steel specimens **a** surface morphology before LSP **b** surface morphology after LSP **c** axial surface topography before LSP and **d** axial surface topography after LSP [128]

with no significant effect on the surface roughness and texture for a wide variety of substrate materials [145]. In addition, WJP as a high-speed water jet provides a constant effect on the workpiece surface [146]. As cold mechanical surface treatment, water jet peening induces localised plastic deformation and compressive stress in the workpiece's surface and near surface layer [147]. This leads to a reduced residual stress especially tensile residual stress and an increase in surface strength and fatigue life hence can be used as preventive maintenance strategies [148]. The WJP process can be used to improve the surface quality of the workpieces with intricate geometries and kerfs with top-notch acuity [149]. In contrast to shot peening, water jet peening is simpler in controlling the water and is lower in terms of cost due to the water preparation. The WJP process is also an environmentally friendly surface treatment process because no dust or other hazardous material is involved during the process [150].

6.1 Working principle of water jet peening

The mechanism of surface treatment in water jet peening occurs due to the impingement of the high-pressure water droplet injected through a nozzle on the treated surface. Figure 40 shows one of the water jet peening experimental setups. A high-pressure water jet produces cavitation, which dissolves after a limited time and releases a strong pressure wave [151]. The strong pressure due to the rupture of the cavitation in the workpiece surface produces a peak load that exceeds the material's yield strength and produces localised plastic deformation confined by the surrounding material. This process generates maximum compressive residual stress on the layer of the workpiece material [150].

The formation of jet's droplets determines the generation of high compressive residual stress in the surface.

Table 6 Comparison on roughness effect of steel and alloy

Ref	*Materials*	R_a *(μm)*	R_z *(μm)*
[6, 7]	304 Stainless steel	0.14	0.16
[8]	NAB alloy	3.27	4.11

Table 7 Comparison of the effect of hardness and residual stress of steel and alloy

Ref	*Materials*	*Hardness (HV)*	*Residual stress (MPa)*
[6]	304 Stainless steel	328	237
[8]	NAB alloy	241	55.8

Table 8 Summary of responses on surfaces and sub-surfaces for various studies in LSP process

Ref	Materials	Parameters	Responses
[114, 120, 129]	304 stainless steel	Direction of laser spot (5 mm — square and round), focal spot size (34 µm), overlapping ratio (25%, 50%, 75%), laser pulse (15 to 25 ns), wavelength (1030 nm), duration (165 fs), pulse energy (up to 1 mJ), laser fluency (30, 40 and 60 J/cm^2)	Stresses are negative
[113, 130]	316L stainless steel	Laser beam diameter (8 mm), peak pressure (2.8 GPa), laser width (50 ns)	Peening impacts increase the magnitude, depth and fatigue crack growth
[131]	TA_{19} alloy	Direction of laser spot (4 mm), energy (30 J/Pulse), frequency (1 Hz), overlapping ratio (15%)	Increases the fatigue crack growth with fatigue crack initiation. Enhanced the fatigue strength around 218%
[115]	Nickel aluminium bronze alloy	Wavelength (1064 nm), energies (0 to 6 J)	Increases residual stresses and surface roughness
[127, 132, 133]	Ti6Al4V	Wavelength (1064 nm), pulse duration (20 ns), spot size (2.4 mm), energy (4 J), overlap rate (50%), temperature (300 °C), laser intensity (4.42 GW/cm^2)	The Micro hardness of the WLSP sample was increased compared to the LSP sample
[115, 134]	Nickel aluminium bronze alloy	Wavelength (1064 nm), energies (0 to 6 J)	Increases residual stresses and surface roughness
[117, 128]	32CrNi high strength low alloy steel	Wavelength (1064 nm), energy (15 J), pulse width (20 ns),	314 MPa at a depth of 0.903 mm. Micro hardness 405 H_V at depth of 0.7 mm
[135]	38CrSi steel	Wavelength (1064 nm), frequency (5 Hz), pulse duration (15 ns), diameter of laser spot (4 mm), overlapping rate (70%)	Surface micro hardness increased. Fatigue life has increased
[136, 137]	Al (7075-T6) alloy- Tic composites	Wavelength (1064 nm), energy (8 J), pulse width (10 ns), frequency of (5 Hz), spot size (1.5 mm), overlapping rate (60%)	Plastic deformation depends upon LSP impact time
[138]	20Cr2Mn2Mo steel alloy	Energies (0 to 8 J), overlapping rate of 50%, carbonitriding (730 & 760 °C),	Temperature affects the roughness and micro hardness in positive
[116]	20Cr2Ni4A alloy steel	Diamond nanoparticles (0.1 mm), wavelength (1064 nm), spot size (3 mm), pulse duration (20 ns), energies (0 to 10 J), frequency of (10 Hz),	Nano-hardness has increased but roughness is in negative
[139]	Mono- and polycrystalline copper	Wavelength (1030 nm), frequency (10 Hz), pulse duration (14 ns), spot size (1.5 × 1.5 mm^2), energy (2.5 J), laser intensity (7.9 GW/cm^2)	Residual stress increases with the density of dislocations
[140]	P/M Ni-based super alloy	Spot size round (2.6 mm), overlapping rate (50%), energy (5 & 7 J)	Increases in fatigue resistance with residual stress in positive
[141, 142]	TIG welded alloy 600 joints	Wavelength (1064 nm), pulse duration (15 ns), energy (25 J), overlapping rate (50%), spot size round (4 mm)	Micro hardness and density of dislocation improved with compressive stress increase
[143]	Aluminized AISI 321 stainless steel	Wavelength (1064 nm), energy (7 J), pulse duration (20 ns), frequency of (2 Hz), overlapping rate (50%), laser intensity (6.59 GW/cm^2)	Fatigue life increased with change in deformation behaviour
[144]	TC6 titanium alloy	Laser intensity (2.6 & 3.6 GW/cm^2), overlapping rate (50%), spot size (4 mm^2)	Improve in fatigue cycle and residual stresses
[110]	Ti-17 titanium alloy	Wavelength (1064 nm), energy (25 J), pulse duration (15 ns), spot size round (4 mm), overlapping rate (50%), laser intensity (13.26 GW/cm^2)	Fatigue crack propagation is reduced with influence in residual stress

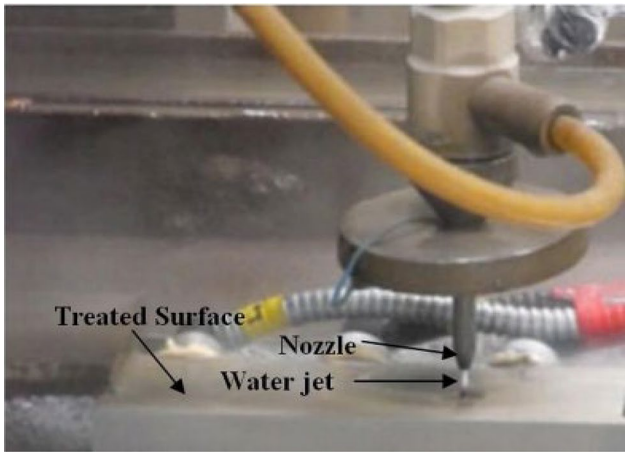

Fig. 40 Experimental setup view of water jet peening [150]

Hence, it is critical to pinpoint the droplet forming area in the jet's configuration and position the workpiece surface in that region [40]. As one of the critical parts in the water jet peening, the jet nozzle design is important. The structure of a jet output from the nozzle, as can be seen in Fig. 41, can be divided into three regions: initial region, transition region, and final region. When the workpiece is positioned in the initial region, a jet produces constant axial dynamic pressure with peak loads below the material's yield strength. As a result, the region is not suitable for the WJP because no plastic deformation occurred. In the transition region, the effect of droplets induces peak loads causing plastic deformation in the impact region. Lastly, in the final region, the droplets dispersed over a wider area, rendering the surface treatment process inefficient. Therefore, the workpiece surface must be located in the main area to achieve the optimum WJP process.

In addition to the distance between the nozzle and the workpiece surface, there are some other parameters and factors affecting the water jet peening process such as standoff distance (SOD), orifice diameter of the nozzle, jet pressure, nozzle feed rate, nozzle angle and exposure time. The typical parameters and their levels are illustrated in Fig. 42 [30, 152].

6.2 Effect of water jet peening on metallic surfaces

Water jet peening is mainly used in metallic surfaces. Some researchers have performed studies on the effect of various water jet peening parameters to the surface and sub-surface quality such as residual stress. Srivastava et al. observed the effect of stand-off distance (SOD) on residual stresses and surface roughness induced by water jet peening process for two types of outlet angles, 0 and 20° [150]. They argued that at smaller SOD, less compressive residual stresses were produced. However, as the distance increased, higher compressive residual stresses were generated to a certain point. Beyond that point, residual stresses were reduced, which implies that the jet was ineffective [148]. Hence, the SOD must be carefully selected to achieve the best residual stress distribution in different pieces [153].

6.2.1 Effect of water jet peening on topography of metallic surface

Some studies have also been performed to observe the effect of water jet peening parameters on the surface roughness. Mochizuki et al. [147] argued that up to a peening time of 15 s, the roughness values are almost identical before and after water peening, resulting in the maximum effect on residual stress [154]. WJP can produce a lower surface roughness as low as 7.2 µm when a large number of jet passes are applied and the slowest feed rate of 1000 mm/min [155]. Fatigue strength of load-free and load-bound surfaces

Fig. 41 Schematic view of jet nozzle [150]

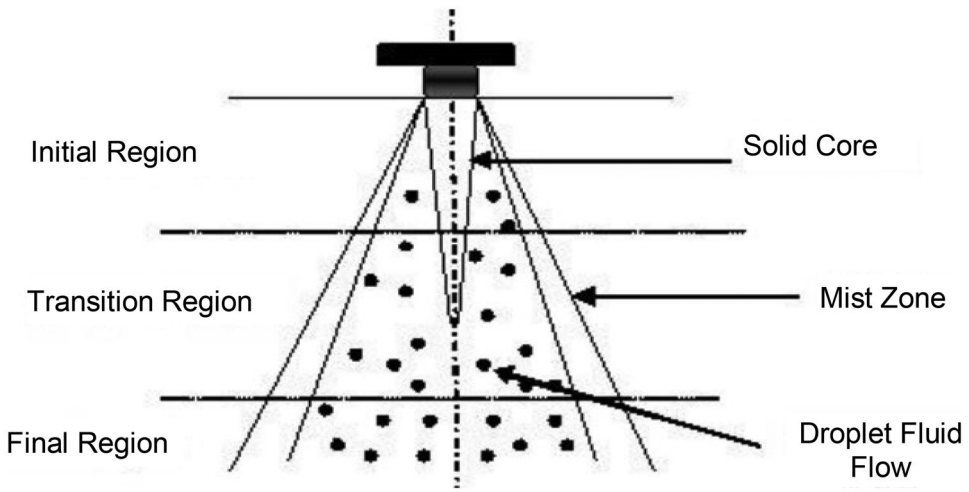

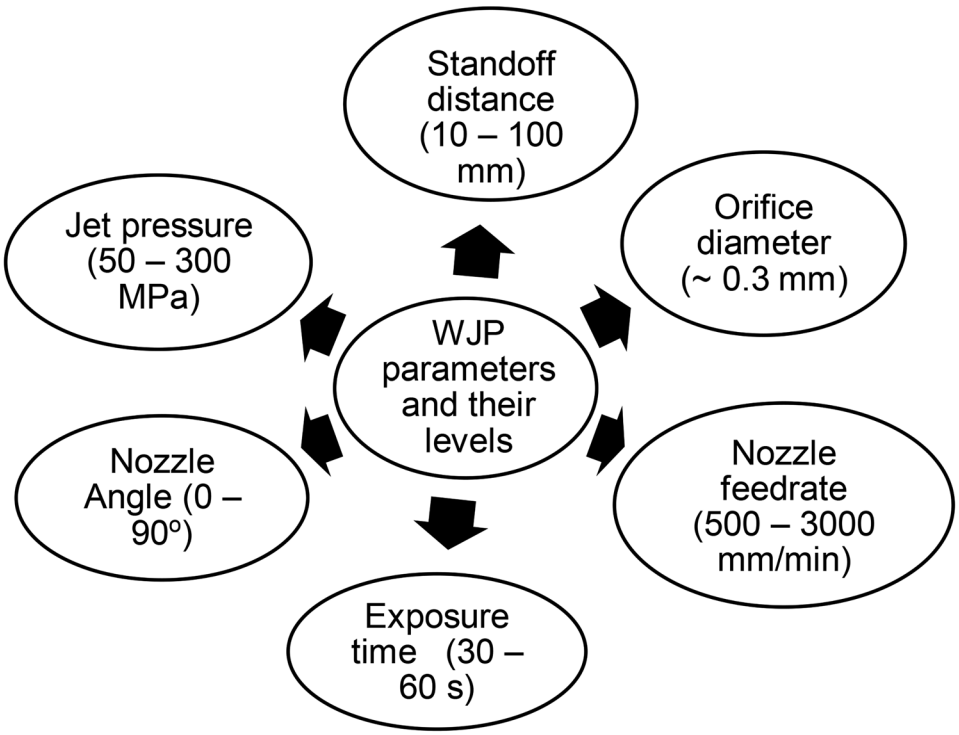

Fig. 42 Typical waterjet peening parameters and their levels

is influenced by surface roughness and topography, and the lack of fatigue resistance is caused by load-free surfaces and high roughness values [146].

The increase of jet pressure can reduce or cut off the erosion from the surface [152]. Strong parameters have been selected to characterise and check viability of abrasive less WJP; water pressure and slow traverse velocity show different effects [155]. The erosion was increased by continuously increasing WJP processing time. The increase of the number of passes and standoff distance increases the surface roughness and friction [156]. Higher standoff distances result in more erosion.

Figure 43a depicts the influence of waterjet peening on surface roughness as a function of the number of passes and the standoff distance. It can be observed that as the number of passes decreases, the arithmetic mean surface roughness (R_a) only exhibits minor improvements at different levels of the standoff distance. Surface roughness, R_a, on the other hand, increases significantly as the standoff interval increases from 20 to 60 mm at the peak number of passes [157].

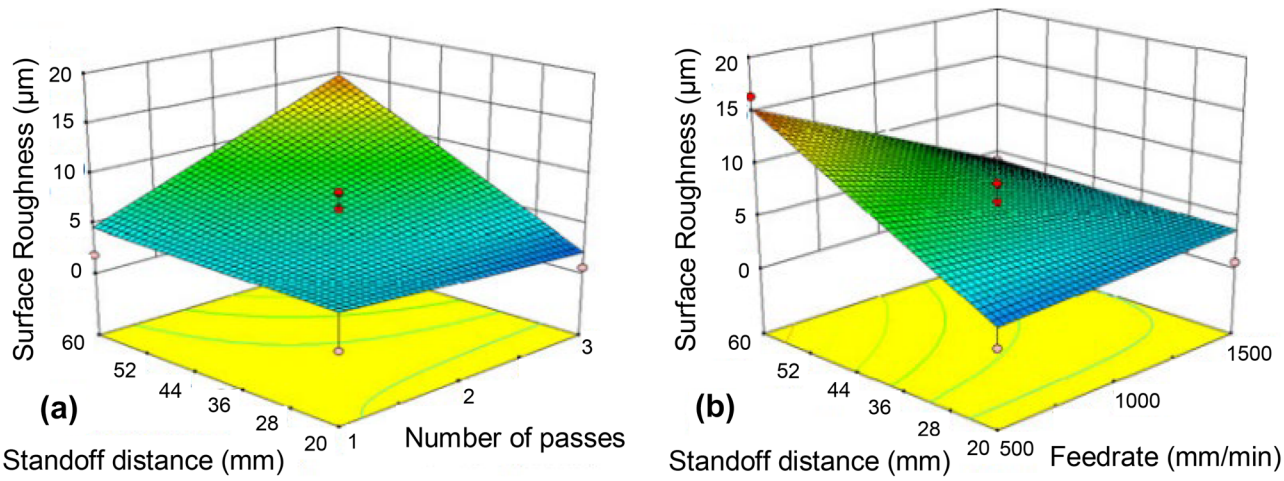

Fig. 43 Effect of waterjet peening on surface roughness for aluminium alloy 5005 specimens **a** interaction between SOD and number of passes and **b** interaction between SOD and feed rate [157]

Table 9 Conditions of different parameters [159]

Conditions	*1–3 passes*	*4–6 passes*	*7–9 passes*
1	300 MPa	-	-
2	300 MPa	200 MPa	-
3	300 MPa	200 MPa	100 MPa

These results imply that the number of passes and the standoff distance has a close relationship, particularly at higher levels of jet passes. Furthermore, the relationship between feed rate and standoff distance indicates a negative influence on surface roughness as shown in Fig. 43b. In some other conditions, the impact of rising the standoff distance on R_a is more noticeable at lower feed rates. At the lowest feed rate, R_a increases dramatically while the standoff distance increases from 20 to 60 mm. Changing the standoff length, on the other side, results in almost no improvement in R_a at the maximum feed rate of 1500 mm/min [158].

It was reported that the additional passes using lower pressure of water jet peening can smoothen the surface from the previous pass [159]. Three conditions were defined as can be seen in Table 9. For each condition, the machining parameters were set to a predefined level accordingly [159].

The roughness parameters for original and three treated surface conditions shown in Table 9 are summarised in Fig. 44. The arithmetic mean roughness value, R_a, has almost the same values for all three conditions implying that surfaces have relatively the same features and profiles [159]. There are, nevertheless, substantial differences in R_z, the average value of the maximum height of the profile, especially between conditions 2 and 3 and condition 1. Conditions 2 and 3 have significantly lower R_z values compared to condition 1. In addition, the R_{pk} (reduced peak height) value also shows a similar trend as R_z values where the treated conditions 2 and 3 appear to be considerably lower than treated condition 1. In contrast, there is no significant difference for the reduced valley depths, R_{vk}, of all conditions [159]. This result implied that the conditions 2 and 3 where lower pressure was applied have successfully smoothen the surface.

6.2.2 Effect of waterjet peening on mechanical properties of metallic surface

The amount of compressive residual stress increases with peening time, reaching a limit of around 560 MPa [27]. The longer peening durations were found to significantly reduce compressive residual stress. The number of passes affects surface roughness, residual stress and hardness. The increase of the number of passes can change the maximum hardness and increase compressive residual stresses [157]. The number of passes affects residual stress depth profiles both in the transverse and longitudinal directions as shown in Fig. 45. The highest surface compressive residual stress was observed in the specimen treated with the most jet passes. The most jet passes also produced the most significant improvement in surface hardness. The insertion of compressive stresses from repetitive water jet impact force is clearly the cause of the increased hardness and thickness of the hardening layer [160].

Pressure is another important variable in the waterjet peening process. The pressure affects residual stresses and roughness. Generally, compressive residual stresses increase by increasing the supply pressure at the beginning, while excessive increase of supply pressure reduces residual stresses significantly [161]. The waterjet peening can improve surface hardness of aluminium alloys AA 6063-T6 of up to 35.9% in [162]. Waterjet peening

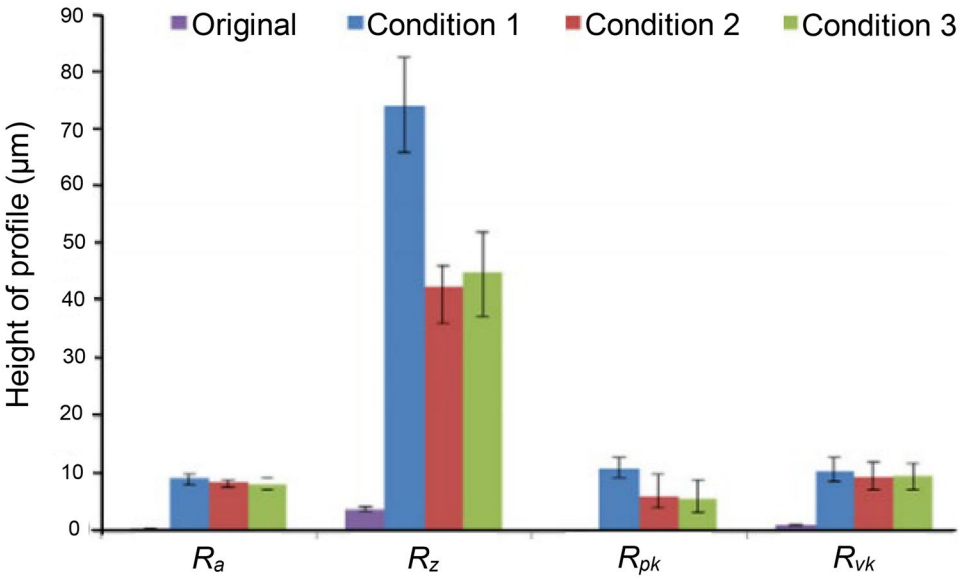

Fig. 44 Roughness parameters of different treated conditions [159]

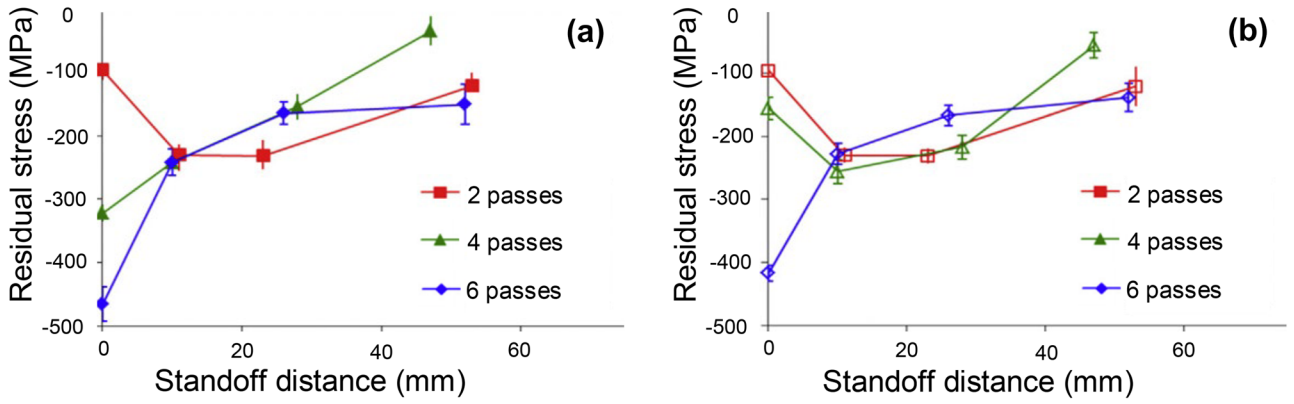

Fig. 45 Residual stress depth profiles for AISI 304 specimens in **a** traverse direction and **b** longitudinal direction [160]

using jet pressure 200 MPa SOD around 100 mm and angle of 20° increases the residual stresses and reduces surface roughness [153]. At a low standoff distance (SOD) of about 10 mm, the compressive residual stress is the highest compared to 20 mm and 30 mm SOD as shown in Fig. 46a [163]. In addition, the low standoff distance also produced the highest hardness [164]. It was observed that there is an increment in hardness from 698 to 1058.34 H_V of a peened sample using parameters of SOD 10 mm and nozzle angle of 45° [164] (Fig. 46b). Peening operations induce compressive residual stress and lead to plastic deformation on the surface. The plastic deformation on the surface is formed by the reduction of d-spacing between two atomic planes. It is important to discuss that waterjet peening enhances the surface hardness by invoking beneficial compressive residual stress induced on the top surface [165].

6.2.3 Effect of waterjet peening on microstructural changes of metallic surface

One of the indications of peening operation is the deposition formation on the substrate which is easily visible in the microstructure. The deposition is formed due to the un-recovered elastic strain from the obstruction of plastic strain. This, subsequently, induces residual strains on the surface layer. The plastic strain on the substrate increases micro hardness and compressive residual stresses so that the fatigue life of the material can be increased [153].

WJP improves the hardness just below the eroded surface from around 210 H_V in the bulk material to around 300 H_V on AISI 316 LVM [145]. The hardening occurred at a depth of around 100 µm. The plastic deformation can be indicated by the changing of the grain size. The sub micrometric/nanometric grains were observed in the 10–20 µm deep below

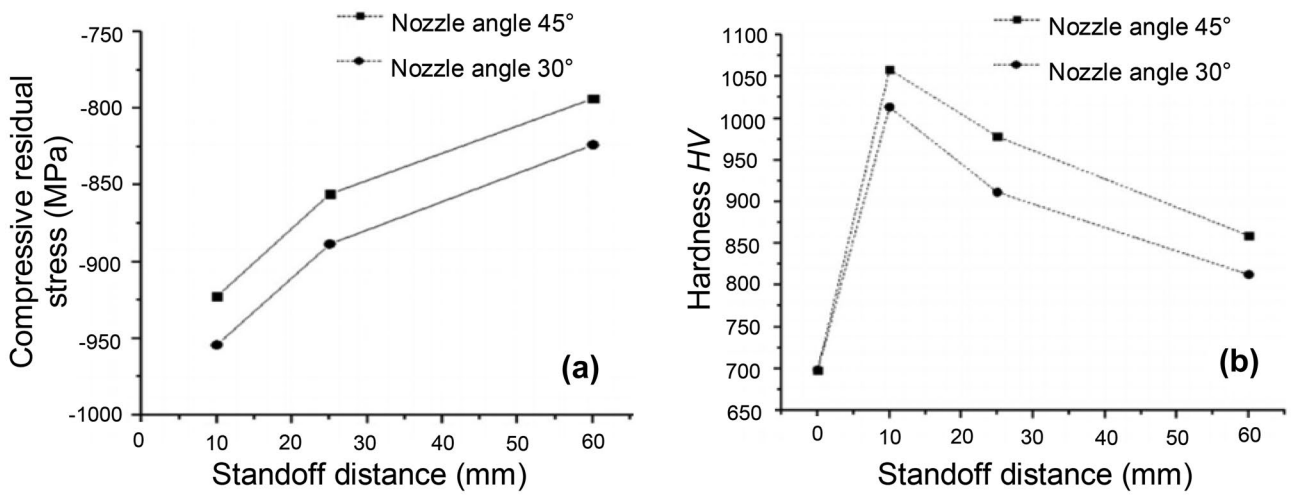

Fig. 46 **a** compressive residual stress for Aluminium alloy 5005 specimens as a function of SOD and nozzle angle [150], and **b** hardness for M2 high speed steel specimens as a function of SOD and nozzle angle [164]

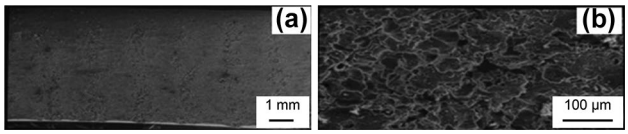

Fig. 47 Surface cavities during WJP for Aluminium alloy 7020-T6 specimens **a** at $P = 100$ MPa and **b** at $P = 200$ MPa [153]

the surface implying that these grains experienced severe plastic deformation [166]. These grain sizes were smaller compared to the grains in the base material which is about 70–100 µm [166]. WJP on AISI 316 LVM produces deeper tracks and undercuts on the surface. The increase of strain resulted in the increase of hardness about 22% and 31% than the base material.

Cavities were produced on the surface due to the waterjet peening (Fig. 47a and b). The higher power supply of about 200 MPa produces more cavities compared to 100 MPa power supplies [153]. The more cavities obviously reduce the fatigue life of the workpiece.

Figure 48 shows a workpiece surface for different treatment conditions. The un-peened surface has a smooth surface finish. The single pass peened surface was seen to have some dull surface and the double passes peened surface produces some ploughing marks (Fig. 48c) implying the existence of deformation degradation on the target substrate's surface [167]. The results on the peened surfaces can occur as an effect of plastic determination, which was induced by a waterjet. The plastic deformation increases the hardness on the peened surface.

Tables 10 and 11 show the surface roughness values, hardness and pressure of two materials, namely stainless steel and aluminium alloy after water jet peening. It can be seen that the surface roughness, especially R_z value of aluminium alloys, is higher compared to stainless steel (Table 10). This can be due to their microstructure [18], less irregular structure and grain presence on the surface of the steel after being treated with water jet peening [148]. Table 11 shows the hardness value of stainless steel which is slightly higher compared to aluminium alloy after the water jet peening at the pressure of 100 MPa. It is indeed that stainless steel has higher hardness compared to aluminium alloys prior to water jet peening. This can occur due to high hardness compressive residual stress of the material and relaxation of material after the waterjet peening [157]. The hardness of the material affects the residual stress during surface treatment [168].

Table 12 shows the summary of the water jet peening processes based on the materials and parameters used and also the key observations. Some research gaps were observed based on this summary such as the application of water jet peening on composites and NFML materials are still rarely discussed.

7 Discussion

Various peening processes have been discussed, especially the effects of the parameters on the surface and sub-surface quality. However, some improvements are still needed based on the reviews and literature study. The advantages and disadvantages of each peening process are summarised in Table 13.

Table 10 Surface roughness of steel and aluminium alloy after water jet peening

Ref	*Materials*	R_a *(µm)*	R_z *(µm)*
[9]	304 austenitic stainless steel	6	7.19
[10]	Aluminium alloy	6.27	16.42

Table 11 Hardness and residual stress of steel and aluminium alloy after water jet peening

Ref	*Materials*	*Hardness* (H_V)	*Residual stress (MPa)*
[9]	304 austenitic stainless steel	120	100
[11, 163]	Aluminium alloy	113.90	89

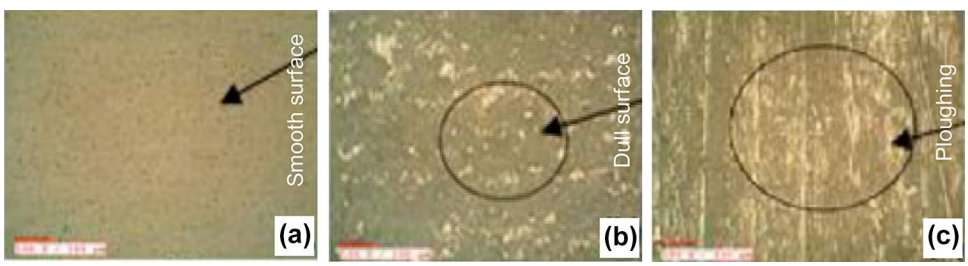

Fig. 48 Micrographs for aluminium alloy 5005 specimens **a** un-peened surface **b** WJP with single pass and **c** WJP with double passes [167]

Table 12 Summary of responses on surfaces and sub-surfaces for various studies in WJP process

Ref	Materials	Parameters	Responses
[161]	18CrNiMo7-6 steel	Pressure (300 MPa), SOD (10 mm), nozzle speed (200 mm/min), carburization (920 °C), quenching (800 °C), tempering (180 °C)	Pressure and hard milling increased the residual stresses
[153]	7020-T6 aluminium	Jet pressure (100 to 200 MPa), SOD (80 to 100 mm), nozzle angle (0 to 20°)	Residual stress 120 MPa, optimum parameters are $P = 150$ MPa, SOD = 80 mm, angle = 20°
[155]	AISI 316 LVM, Ti6Al4V	Pressure (360 MPa), velocities (0.05 and 0.1 m/min)	AISI 316 LVM has deeper tracks and deeper undercuts compared to Ti6Al4V
[154]	16 MnCr5E	Pressure (75 MPa), angle (10°), peening time (0.5 s)	Structural disturbances are approximately constant at about 900 MPa
[162]	AA 6063-T6	Pressure (150 to 170 MPa), SOD (80 to 100 mm)	The surface roughness of the peened sample was improved
[18]	Austenitic stainless steel 304	Nozzle diameter 0.3 mm, angle (90°), number of passes (2, 4, 6), feed rate (1000 to 3000 mm/min), pressure (100 to 300 MPa),	An increase in feed rate and pressure affects the hardness
[157]	Aluminium alloy 5005	Nozzle diameter (0.3 mm), angle (90°), passes (1, 2, 3), pressure (50, 100, 150 MPa), feed rate (500, 1000, 1500 mm/min), SOD (20, 40, 60 mm)	An increase in pressure from 50 to 150 MPa has affected the stresses and hardness
[168, 169]	Al6061-T6	Jet velocity (0.86 m/s), angle (90°), SOD (3 mm), nozzle diameter (0.3 mm)	Waterjet peening increases fatigue growth
[170]	Carbon steel 1045	Number of passes (2, 4, 6), pressure (100—300 MPa)	High surface roughness and erosion improved in hardness and damage in grain
[171]	Aluminium–lithium 8090 alloy	Flow rate (14 L/min), SOD (100 mm), pressure (50 MPa), nozzle diameter (1.5 mm), time (20 min), angle (20°)	Hardness, surface roughness, and erosion increased

Table 13 Comparison of all peening processes (SP, LSP and WJP)

Process	Advantages	Disadvantages
Shot Peening	• Cold process and easy to control [172] • Wide parameters range • Every type of substrate would be used • Shots can improve thin depth residual stress [57] • Peened components are mainly strain hardening due to multiple shots [174] • Strain rate of small and light shots should be high, leading to more surface defects [175] • Show durability on material • Stave off common damage such as cracking, galling, and fretting [173]	• Limited with depth 0.25 mm maximum [57] • Fatigue resistance limited [39] • Random area dispersal • Welded component restrictions for process [41] • Less affected on deformation behaviour [71] • Erosion and corrosion hasn't well treated [88]
Laser shock peening	• Operate at high temperature [121] • Maintain residual stresses at high temperature [114] • Maintain residual stresses at depth up to 1–2 mm [139] • Superior fatigue resistance [120] • Increase life of welded components [110] • Severe plastically deformed region exhibited residual compressive stress[176] • No process contamination • Topography easily maintained and control [36]	• Need high energy for process [121] • Limited range of parameters • Limited substrate, and material has process • Thin surface dominate in residual stress [79] • Distortion in the peened components[176] • High strain rate response is caused in the material [177] • Higher crack length affects the LSP performance
Waterjet peening	• Cold process and environment-friendly [79] • Wide range of working parameters • Easily access critical and less-access area [18] • Plastic strain is more on ductile material [178] • Full coverage of treated area • Excellent resistance on corrosion and erosion [171] • Good resistance to fatigue strength with micro-cracks	• Working parameters must be optimised to avoid damage • Limited substrate and material have the process • Micro strain has destruction by introducing compressive residual stress[179] • Roughness has not treated well [155] • Severe risk over abrasion

8 Conclusion

The study on the various peening processes shows the potential to improve surface and sub-surface quality of the peened components. The peening process is known as one of the treatments to improve the quality of the engineering materials. Three peening processes are reviewed and discussed in this paper. They are shot peening, laser shock peening and water jet peening. The working principles of the three peening processes are explained and discussed. The effect of these processes on the surface topography, mechanical properties and microstructural conditions for various materials, setups and parameters are explored and highlighted. Selections of the optimum peening parameters are significant in order to achieve good quality in terms of surface topography, surface and sub-surface mechanical properties and sub-surface microstructural conditions. The challenges to produce compressive residual stress and extend the fatigue life for engineering components have also been investigated and reported. Finally, this paper has summarised the advantages and disadvantages of the three peening processes. This summary is important for researchers and engineers in selecting the correct and suitable process for their applications.

Acknowledgements Authors would like to gratefully acknowledge the financial support from the Ministry of Higher Education Malaysia through FRGS/1/2019/TK03/UMP/02/25 and Universiti Malaysia Pahang through RDU1901161.

Author contribution Syed Qutaba: conceptualization, methodology, literature review, analysis and writing. Mebrahitom Asmelash: conceptualization, methodology, collecting the data and writing — original draft. Kushendarsyah Saptaji: conceptualization, review paper citation, administration and drafting. Azmir Azhari: conceptualization, methodology, design layout, review, funding acquisition, and supervision.

Funding The financial support is from the Ministry of Higher Education Malaysia through FRGS/1/2019/TK03/UMP/02/25, Universiti Malaysia Pahang through RDU1901161 and UMP Doctoral research scheme funds.

Declarations

Ethics approval Not applicable.

Consent to participate Not applicable.

Consent for publication Not applicable.

Competing interests The authors declare no competing interests.

References

1. Özdemir A, Kocabaş İ, Svanda P (2016) Improving the strength of adhesively bonded joints through the introduction of various surface treatments. J Adhes Sci Technol 30:2573–2595. https://doi.org/10.1080/01694243.2016.1188872
2. Cooper L, Benhaddad S, Wood A, Ivey DG (2008) The effect of surface treatment on the oxidation of ferritic stainless steels used for solid oxide fuel cell interconnects. J Power Sources 184:220–228. https://doi.org/10.1016/j.jpowsour.2008.06.010
3. Han S-H, Han J-W, Nam Y-Y, Cho I-H (2009) Fatigue life improvement for cruciform welded joint by mechanical surface treatment using hammer peening and UNSM. In: Engineering against fracture. Springer, pp 411–419
4. Xianghuai L (2000) Recent advance in surface treatment and its applications in China. Surf Coatings Technol 131:261–266. https://doi.org/10.1016/s0257-8972(00)00791-x
5. Han J, Niu H, Li S et al (2020) Effect of mechanical surface treatment on the bonding mechanism and properties of cold-rolled Cu/Al clad plate. Chinese J Mech Eng 33(1):1-13. https://doi.org/10.1186/s10033-020-00483-x
6. Ulutan D, Ozel T (2011) Machining induced surface integrity in titanium and nickel alloys: a review. Int J Mach Tools Manuf 51:250–280. https://doi.org/10.1016/j.ijmachtools.2010.11.003
7. Todaka Y, Umemoto M, Tsuchiya K (2004) Comparison of nanocrystalline surface layer in steels formed by air blast and ultrasonic shot peening. Mater Trans 45:376–379. https://doi.org/10.2320/matertrans.45.376
8. Schulze V (2006) Modern mechanical surface treatment: states, stability, effects. John Wiley & Sons
9. Zhang T, Liu X, Zhang N (2014) Analysis of antiwear for hydraulic relief valves under different surface treatment processes. Mater Res Innov 18:S1–5-S1–7. https://doi.org/10.1179/1432891713z.000000000360
10. Primee S, Juijerm P (2019) Modified mechanical surface treatment for optimized fatigue performance of martensitic stainless steel AISI 420. Met Mater Int 27:946–952. https://doi.org/10.1007/s12540-019-00517-7
11. Mart´ınez PF (2012) Diffusion through oxide barriers for solar cell applications. University of Konstanz
12. Pathak C, Dodkar P (2020) Effect of Shot Blasting and Shot Peening Parameters on Residual Stresses Induced in Connecting Rod. Trans Indian Inst Met 73:571–576. https://doi.org/10.1007/s12666-020-01866-3
13. Hanawa T (2015) Functionalisation of metallic surfaces for biomedical applications. Surf. Coat. Modif. Met. Biomater. 275–286
14. Kloos KH, Macherauch E (1987) Development of mechanical surface strengthening processes from the beginning until today. (Retroactive Coverage). Shot Peen Sci Technol 3–27
15. Bleicher F, Lechner C, Habersohn C et al (2012) Mechanism of surface modification using machine hammer peening technology. CIRP Ann 61:375–378. https://doi.org/10.1016/j.cirp.2012.03.139
16. Schulze V, Bleicher F, Groche P et al (2016) Surface modification by machine hammer peening and burnishing. CIRP Ann 65:809–832. https://doi.org/10.1016/j.cirp.2016.05.005
17. Kirk D (1999) Shot peening Aircr Eng Aerosp Technol 71:349–361. https://doi.org/10.1108/00022669910270727
18. Azhari A, Schindler C, Kerscher E, Grad P (2012) Improving surface hardness of austenitic stainless steel using waterjet peening process. Int J Adv Manuf Technol 63:1035–1046. https://doi.org/10.1007/s00170-012-3962-1
19. Grinspan AS, Gnanamoorthy R (2006) A novel surface modification technique for the introduction of compressive residual stress and preliminary studies on Al alloy AA6063. Surf Coatings Technol 201:1768–1775. https://doi.org/10.1016/j.surfcoat.2006.03.002
20. Gao Y-K, Yao M, Shao P-G, Zhao Y-H (2003) Another mechanism for fatigue strength improvement of metallic parts by shot peening. J Mater Eng Perform 12:507–511. https://doi.org/10.1361/105994903100277148
21. Omari MA, Mousa HM, AL-Oqla FM, Aljarrah M, (2019) Enhancing the surface hardness and roughness of engine blades using the shot peening process. Int J Miner Metall Mater 26:999–1004. https://doi.org/10.1007/s12613-019-1818-5
22. Manufacturing Guide Sweden AB (2014) Hot Rolling of sheets. https://www.manufacturingguide.com/en/hot-rolling-sheets. Accessed 25 Jul 2021
23. Chi G, Hu S, Yang Y, Chen T (2012) Response surface methodology with prediction uncertainty: a multi-objective optimisation approach. Chem Eng Res Des 90:1235–1244. https://doi.org/10.1016/j.cherd.2011.12.012
24. Zhao C, Gao Y, Guo J et al (2015) Investigation on residual stress induced by shot peening. J Mater Eng Perform 24:1340–1346. https://doi.org/10.1007/s11665-014-1382-0
25. Chan WL, Cheng HKF (2022) Hammer peening technology—the past, present, and future. Int J Adv Manuf Technol 118:683–701. https://doi.org/10.1007/s00170-021-07993-5
26. Torres MAS, do Nascimento MP, Voorwald HJC (2002) Consideration of shot peening treatment applied to a high strength aeronautical steel with different hardness. Shot Peen 37–43
27. Chillman A, Ramulu M, Hashish M (2007) Waterjet peening and surface preparation at 600 MPa: A preliminary experimental study
28. Lee H, Kim D, Jung J et al (2009) Influence of peening on the corrosion properties of AISI 304 stainless steel. Corros Sci 51:2826–2830. https://doi.org/10.1016/j.corsci.2009.08.008
29. Bagheri S, Guagliano M (2009) Review of shot peening processes to obtain nanocrystalline surfaces in metal alloys. Surf Eng 25:3–14. https://doi.org/10.1179/026708408x334087
30. Chillman A, Ramulu M, Hashish M (2010) Waterjet and Water-Air Jet Surface Processing of a Titanium Alloy: A Parametric Evaluation. J Manuf Sci Eng 132. https://doi.org/10.1115/1.4000837
31. Toppo A, Kaul R, Pujar MG et al (2012) Enhancement of corrosion resistance of type 304 stainless steel through a novel thermo-mechanical surface treatment. J Mater Eng Perform 22:632–639. https://doi.org/10.1007/s11665-012-0304-2
32. Shaw BA, Aylott C, O'hara P, Brimble K (2003) The role of residual stress on the fatigue strength of high performance gearing. Int J Fatigue 25:1279–1283
33. Chen JS, Desai DA, Heyns SP, Pietra F (2019) Literature review of numerical simulation and optimisation of the shot peening process. Adv Mech Eng 11:168781401881827. https://doi.org/10.1177/1687814018818277
34. Meguid SA (1991) Effect of partial-coverage upon the fatigue fracture behaviour of peened components. Fatigue Fract Eng Mater Struct 14:515–530
35. Hong T, Ooi JY, Shaw B (2008) A numerical simulation to relate the shot peening parameters to the induced residual stresses. Eng Fail Anal 15:1097–1110. https://doi.org/10.1016/j.engfailanal.2007.11.017
36. Alam MM, Barsoum Z, Jonsén P et al (2010) The influence of surface geometry and topography on the fatigue cracking behaviour of laser hybrid welded eccentric fillet joints. Appl Surf Sci 256:1936–1945. https://doi.org/10.1016/j.apsusc.2009.10.041
37. Davim JP (2011) Tribology for engineers: a practical guide, 1st edn. Woodhead Publishing Ltd, Cambridge
38. Zabeen S, Preuss M, Withers PJ (2015) Evolution of a laser shock peened residual stress field locally with foreign object damage and subsequent fatigue crack growth. Acta Mater 83:216–226. https://doi.org/10.1016/j.actamat.2014.09.032

39. Guagliano M, Vergani L (2004) An approach for prediction of fatigue strength of shot peened components. Eng Fract Mech 71:501–512. https://doi.org/10.1016/s0013-7944(03)00017-1
40. Daniewicz SR, Cummings SD (1999) Characterization of a water peening process. J Eng Mater Technol 121:336–340. https://doi.org/10.1115/1.2812383
41. Lostado Lorza R, Escribano García R, Martínez Calvo M, Múgica Vidal R (2016) Improvement in the design of welded joints of EN 235JR low carbon steel by multiple response surface methodology. Metals (Basel) 6:205. https://doi.org/10.3390/met6090205
42. Widodo TD, Noda K (2013) Corrosion resistance enhancement of 304 stainless steel under droplet of chloride solution by mechanical surface treatment. Proc. 8th Pacific Rim Int. Congr. Adv. Mater. Process. 2423–2429
43. Tagliari M dos R, Antunes MR, Santos JGN dos et al (2019) Tensile armor wires submitted to slow strain rate tests in a corrosive environment and cathodic protection: a comparison between two different microstructures. Mater Res 22:
44. Bagheri Fard S, Guagliano M (2009) Effects of surfaces nanocrystallization induced by shot peening on material properties : a review. Frat ed Integrità Strutt 3:3–16. https://doi.org/10.3221/igf-esis.07.01
45. Xin H, Correia JAFO, Veljkovic M et al (2021) Residual stress effects on fatigue life prediction using hardness measurements for butt-welded joints made of high strength steels. Int J Fatigue 147:106175. https://doi.org/10.1016/j.ijfatigue.2021.106175
46. James MN, Newby M, Hattingh DG, Steuwer A (2010) Shot-peening of steam turbine blades: residual stresses and their modification by fatigue cycling. Procedia Eng 2:441–451. https://doi.org/10.1016/j.proeng.2010.03.048
47. Ding X, Kang Y, Li D et al (2017) Experimental investigation on surface quality processed by self-excited oscillation pulsed waterjet peening. Mater. 10
48. Nissan AB, Findley KO (2014) 12.16 - microstructures and mechanical performance of induction-hardened medium-carbon steels. In: Hashmi S, Batalha GF, Van Tyne CJ, Yilbas BBT-CMP (eds). Elsevier, Oxford, pp 581–604
49. Guo P, Zhao Y, Zeng W, Hong Q (2013) The effect of microstructure on the mechanical properties of TC4-DT titanium alloys. Mater Sci Eng A 563:106–111. https://doi.org/10.1016/j.msea.2012.11.033
50. Cui CY, Wan TY, Shu YX et al (2019) Microstructure evolution and mechanical properties of aging 6061 Al alloy via laser shock processing. J Alloys Compd 803:1112–1118. https://doi.org/10.1016/j.jallcom.2019.06.347
51. Turski M, Clitheroe S, Evans AD et al (2010) Engineering the residual stress state and microstructure of stainless steel with mechanical surface treatments. Appl Phys A 99:549–556. https://doi.org/10.1007/s00339-010-5672-6
52. Wang TS, Lu B, Zhang M et al (2007) Nanocrystallization and α martensite formation in the surface layer of medium-manganese austenitic wear-resistant steel caused by shot peening. Mater Sci Eng A 458:249–252. https://doi.org/10.1016/j.msea.2006.12.066
53. Ni Z, Wang X, Wang J, Wu E (2003) Characterization of the phase transformation in a nanostructured surface layer of 304 stainless steel induced by high-energy shot peening. Phys B Condens Matter 334:221–228. https://doi.org/10.1016/S0921-4526(03)00069-3
54. Nascimento MP, Souza RC, Pigatin WL, Voorwald HJC (2001) Effects of surface treatments on the fatigue strength of AISI 4340 aeronautical steel. Int J Fatigue 23:607–618
55. Papenberg NP, Gneiger S, Weißensteiner I et al (2020) Mg-alloys for forging applications—a review. Mater. 13
56. Dalaei K, Karlsson B, Svensson L-E (2011) Stability of shot peening induced residual stresses and their influence on fatigue lifetime. Mater Sci Eng A 528:1008–1015
57. Pariente IF, Guagliano M (2009) Influence of shot peening process on contact fatigue behavior of gears. Mater Manuf Process 24:1436–1441. https://doi.org/10.1080/10426910903386097
58. George PM, Pillai N, Shah N (2004) Optimization of shot peening parameters using Taguchi technique. J Mater Process Technol 153–154:925–930. https://doi.org/10.1016/j.jmatprotec.2004.04.159
59. Miao HY (2010) Numerical and theoretical study of shot peening and stress peen forming process. University of Montreal
60. Gariépy A, Larose S, Perron C et al (2013) On the effect of the peening trajectory in shot peen forming. Finite Elem Anal Des 69:48–61
61. Hashemi B, Rezaee Yazdi M, Azar V (2011) The wear and corrosion resistance of shot peened–nitrided 316L austenitic stainless steel. Mater Des 32:3287–3292. https://doi.org/10.1016/j.matdes.2011.02.037
62. Fragoudakis R, Saigal A, Savaidis G et al (2013) Fatigue assessment and failure analysis of shot-peened leaf springs. Fatigue Fract Eng Mater Struct 36:92–101
63. Xu LD, Sun XY, Wan P et al (2015) Surface treatment of interfacial properties of shape memory alloy composites. Mater Res Innov 19:S5–734-S5–738. https://doi.org/10.1179/1432891714z.0000000001184
64. Girish DV, Mayuram MM, Krishnamurthy S (1996) Surface integrity studies on shot-peened thermal-treated En 24 steel spur gears. Wear 193:242–247. https://doi.org/10.1016/0043-1648(95)06791-4
65. Wang C, Li W, Jiang J et al (2021) A new methodology to establish the relationship between equivalent shot velocity and air pressure by surface roughness for shot peening. Int J Adv Manuf Technol 112:2233–2247. https://doi.org/10.1007/s00170-020-06423-2
66. Thielen S, Breuninger P, Hotz H et al (2021) Improving the tribological properties of radial shaft seal counter surfaces using experimental micro peening and classical shot peening processes. Tribol Int 155:106764. https://doi.org/10.1016/j.triboint.2020.106764
67. Atieh AM, Rawashdeh NA, AlHazaa AN (2018) Evaluation of surface roughness by image processing of a shot-peened, TIG-welded aluminum 6061–T6 alloy: an experimental case study. Materials (Basel) 11:771
68. Benedetti M, Bortolamedi T, Fontanari V, Frendo F (2004) Bending fatigue behaviour of differently shot peened Al 6082 T5 alloy. Int J Fatigue 26:889–897
69. Ramana EV, Reddy PR (2013) Optimization of shot peening process parameters using Taguchi approach and validation by data mining. Int J Eng Sci Technol 5:1471
70. Bassindale C, Miller RE, Wang X (2020) Effect of single initial overload and mean load on the low-cycle fatigue life of normalized 300 M alloy steel. Int J Fatigue 130:105273
71. Nascimento MP, Torres MAS, Souza RC, Voorwald HJC (2002) Effect of a shot peening pre treatment on the fatigue behaviour of hard chromium on electroless nickel interlayer coated AISI 4340 aeronautical steel. Mater Res 5:95–100. https://doi.org/10.1590/s1516-14392002000200002
72. Soyama H, Chighizola CR, Hill MR (2021) Effect of compressive residual stress introduced by cavitation peening and shot peening on the improvement of fatigue strength of stainless steel. J Mater Process Technol 288:116877. https://doi.org/10.1016/j.jmatprotec.2020.116877
73. Lin Q, Liu H, Zhu C et al (2020) Effects of different shot peening parameters on residual stress, surface roughness and cell size. Surf Coatings Technol 398:126054. https://doi.org/10.1016/j.surfcoat.2020.126054
74. Wu J, Liu H, Wei P et al (2020) Effect of shot peening coverage on hardness, residual stress and surface morphology of

carburized rollers. Surf Coatings Technol 384:125273. https://doi.org/10.1016/j.surfcoat.2019.125273
75. Yang Q, Zhou W, Niu Z et al (2018) Effect of different surface asperities and surface hardness induced by shot-peening on the fretting wear behavior of Ti-6Al-4V. Surf Coatings Technol 349:1098–1106. https://doi.org/10.1016/j.surfcoat.2018.06.092
76. Liu ZG, Wong TI, Huang W et al (2017) Effect of surface polishing treatment on the fatigue performance of shot-peened Ti–6Al–4V alloy. Acta Metall Sin English Lett 30:630–640. https://doi.org/10.1007/s40195-017-0555-x
77. Zhu K, Jiang C, Li Z et al (2016) Residual stress and microstructure of the CNT/6061 composite after shot peening. Mater Des 107:333–340. https://doi.org/10.1016/j.matdes.2016.06.030
78. Rotundo F, Korsunsky AM (2009) Synchrotron XRD study of residual stress in a shot peened Al/SiCp composite. Procedia Eng 1:221–224. https://doi.org/10.1016/j.proeng.2009.06.052
79. Azhari A, Sulaiman S, Rao AKP (2016) A review on the application of peening processes for surface treatment. IOP Conf Ser Mater Sci Eng 114:12002. https://doi.org/10.1088/1757-899x/114/1/012002
80. Kulkarni L, Kulkarni V (2014) Effect of shot velocity on residual stresses in shot peening. Int J Eng Res Technol 3:1284–1287
81. Nakonieczny A, Monka G (2013) Contact fatigue strength of 41CrAlMo7 grade steel under nitriding and shot-peening treatment. Mater Sci 48:715–721. https://doi.org/10.1007/s11003-013-9559-5
82. Jung JS, Pyoun Y, Cho I (2009) Effect of ultrasonic and air blast shot peening on the microstructural evolution and mechanical properties of SUS304. J Korean Phys Soc 54(3)
83. Li H, Lu Y, Han Z, Guo X, Xu Y, Xu X, Tao J (2019) The shot peen forming of fiber metal laminates based on the aluminum-lithium alloy: Deformation characteristics. Composites Part B: Engineering, 158, 279-285
84. Zhu K, Li Z, Fan G et al (2019) Thermal relaxation of residual stress in shot-peened CNT/Al–Mg–Si alloy composites. J Mater Res Technol 8:2201–2208. https://doi.org/10.1016/j.jmrt.2019.01.023
85. Zhang R, Han B, Wang Y (2015) Strengthening of ultra high-temperature ceramics by shot peening and multiple crack healing. Mater Lett 160:132–134. https://doi.org/10.1016/j.matlet.2015.07.064
86. Wu J, Wei P, Liu H et al (2021) Realization of various shot peening intensities and its effect on surface integrity of 18CrNiMo7–6 steel. Surf Coatings Technol 127194
87. Peral LB, Quintero A, Vielma AT et al (2021) TEM evaluation of steel nanocrystalline surfaces obtained by severe shot peening. Surf Coatings Technol 418:127238. https://doi.org/10.1016/j.surfcoat.2021.127238
88. Rajesh A, Ashoka Varthanan P, Srikant J et al (2021) Optimization of shot peening process parameters using PSO algorithm to maximise the fatigue strength, flexural strength and surface hardness of AA2024-T3 alloy. Mater Today Proc. https://doi.org/10.1016/j.matpr.2020.12.1073
89. Wen Y, Wu Y, Hua L et al (2021) Effects of shot peening on microstructure evolution and mechanical properties of surface nanocrystal layer on titanium matrix composite. Mater Des 206:109760. https://doi.org/10.1016/j.matdes.2021.109760
90. Liu H, Chen M, Wang L et al (2019) Investigation on microstructure and properties of Al18B4O33 whisker reinforced Al Mg Si matrix composite after shot peening. Vacuum 160:303–310. https://doi.org/10.1016/j.vacuum.2018.11.031
91. Cao Z, Xu H, Zou S, CHE Z (2012) Investigation of Surface Integrity on TC17 Titanium Alloy Treated by Square-spot Laser Shock Peening. Chinese J Aeronaut 25:650–656. https://doi.org/10.1016/s1000-9361(11)60429-9
92. Huang S, Agyenim-Boateng E, Sheng J et al (2019) Effects of laser peening with different laser power densities on the mechanical properties of hydrogenated TC4 titanium alloy. Int J Hydrogen Energy 44:17114–17126. https://doi.org/10.1016/j.ijhydene.2019.05.002
93. Brett SJ, Mitchell KC (2012) Welding and repair technology for power plants. In: Proc. 10th Int. EPRI Conf., EPRI Marco Island, FL, USA. pp 1–14
94. Liao Y, Ye C, Cheng GJ (2016) [INVITED] A review: warm laser shock peening and related laser processing technique. Opt Laser Technol 78:15–24. https://doi.org/10.1016/j.optlastec.2015.09.014
95. Im J, Grandhi RV, Ro Y (2012) Residual stress behaviors induced by laser peening along the edge of curved models. J Mech Sci Technol 26:3943–3952. https://doi.org/10.1007/s12206-012-0913-6
96. Li J, Zhou J, Feng A et al (2018) Analysis of microstructure and tensile properties produced by cryogenic laser peening on 2024–T351 aluminum alloy. Vacuum 158:141–145
97. Ding K, Ye L (2006) Simulation of multiple laser shock peening of a 35CD4 steel alloy. J Mater Process Technol 178:162–169. https://doi.org/10.1016/j.jmatprotec.2006.03.170
98. Toparli MB, Fitzpatrick ME, Gungor S (2013) Improvement of the contour method for measurement of near-surface residual stresses from laser peening. Exp Mech 53:1705–1718. https://doi.org/10.1007/s11340-013-9766-x
99. Kulekci MK, Esme U (2014) Critical analysis of processes and apparatus for industrial surface peening technologies. Int J Adv Manuf Technol 74:1551–1565. https://doi.org/10.1007/s00170-014-6088-9
100. Spadaro L, Gomez-Rosas G, Rubio-González C et al (2017) Fatigue behavior of superferritic stainless steel laser shock treated without protective coating. Opt Laser Technol 93:208–215
101. Montross CS, Wei T, Ye L et al (2002) Laser shock processing and its effects on microstructure and properties of metal alloys: a review. Int J Fatigue 24:1021–1036
102. Sathyajith S, Kalainathan S, Swaroop S (2013) Laser peening without coating on aluminum alloy Al-6061-T6 using low energy Nd:YAG laser. Opt Laser Technol 45:389–394. https://doi.org/10.1016/j.optlastec.2012.06.019
103. Yong CK, West GD, Gibbons GJ, Wong CC (2019) Influence of laser shock peening (LSP) on the material properties of additive manufactured IN718. In: International Conference on Advanced Surface Enhancement. Springer, pp 305–313
104. Maawad E, Sano Y, Wagner L et al (2012) Investigation of laser shock peening effects on residual stress state and fatigue performance of titanium alloys. Mater Sci Eng A 536:82–91. https://doi.org/10.1016/j.msea.2011.12.072
105. Wu LJ, Luo KY, Liu Y et al (2018) Effects of laser shock peening on the micro-hardness, tensile properties, and fracture morphologies of CP-Ti alloy at different temperatures. Appl Surf Sci 431:122–134. https://doi.org/10.1016/j.apsusc.2017.05.202
106. Wang C, Li K, Hu X et al (2021) Numerical study on laser shock peening of TC4 titanium alloy based on the plate and blade model. Opt Laser Technol 142:107163. https://doi.org/10.1016/j.optlastec.2021.107163
107. Xiang YF, Mei RL, Wang SP et al (2021) Numerical investigation of the effect of laser shock peening parameters on the residual stress and deformation response of 7075 aluminum alloy. Optik (Stuttg) 243:167446. https://doi.org/10.1016/j.ijleo.2021.167446
108. Ding H, Shin YC (2012) Dislocation density-based modeling of subsurface grain refinement with laser-induced shock compression. Comput Mater Sci 53:79–88. https://doi.org/10.1016/j.commatsci.2011.08.038
109. Gonzalez-Romero R, Strojnik M, Garcia-Torales G, Gomez-Rosas G (2021) Frequency dependence of a piezo-resistive method for pressure measurements of laser-induced shock waves

in solids. In: Photonics. Multidisciplinary Digital Publishing Institute, p 120
110. Sun R, Keller S, Zhu Y et al (2021) Experimental-numerical study of laser-shock-peening-induced retardation of fatigue crack propagation in Ti-17 titanium alloy. Int J Fatigue 145:106081. https://doi.org/10.1016/j.ijfatigue.2020.106081
111. Peyre P, Fabbro R, Merrien P, Lieurade HP (1996) Laser shock processing of aluminium alloys. Application to high cycle fatigue behaviour. Mater Sci Eng A 210:102–113. https://doi.org/10.1016/0921-5093(95)10084-9
112. Li K, Cai Y, Yu Z, Hu J (2020) Formation mechanism of residual stress hole under different pulse durations and shock pressure distributions in Ti6Al4V alloy during laser peen texturing. Opt Laser Technol 130:106361. https://doi.org/10.1016/j.optlastec.2020.106361
113. Bikdeloo R, Farrahi GH, Mehmanparast A, Mahdavi SM (2020) Multiple laser shock peening effects on residual stress distribution and fatigue crack growth behaviour of 316L stainless steel. Theor Appl Fract Mech 105:102429. https://doi.org/10.1016/j.tafmec.2019.102429
114. HU Y, YAO Z (2008) Fem simulation of residual stresses induced by laser shock with overlapping laser spots. Acta Metall Sin English Lett 21:125–132. https://doi.org/10.1016/s1006-7191(08)60029-0
115. Gao Y, Yang W, Huang Z, Lu Z (2021) Effects of residual stress and surface roughness on the fatigue life of nickel aluminium bronze alloy under laser shock peening. Eng Fract Mech 244:107524. https://doi.org/10.1016/j.engfracmech.2021.107524
116. Lu H, Ren Y, Chen Y et al (2021) Wear resistance of 20Cr2Ni4A alloy steel treated by laser shock peening and implantation of diamond nanoparticles. Surf Coatings Technol 412:127070. https://doi.org/10.1016/j.surfcoat.2021.127070
117. Yong W, Xibin W, Zhibing L et al (2020) Effects of laser shock peening in different processes on fatigue life of 32CrNi steel. Mater Sci Eng A 796:139933
118. Nemat-Nasser S, Guo WG, Cheng JY (1999) Mechanical properties and deformation mechanisms of a commercially pure titanium. Acta Mater 47:3705–3720. https://doi.org/10.1016/s1359-6454(99)00203-7
119. Ye C, Suslov S, Kim BJ et al (2011) Fatigue performance improvement in AISI 4140 steel by dynamic strain aging and dynamic precipitation during warm laser shock peening. Acta Mater 59:1014–1025. https://doi.org/10.1016/j.actamat.2010.10.032
120. Li Y, Ren Z, Jia X et al (2021) The effects of the confining medium and protective layer during femtosecond laser shock peening. Manuf Lett 27:26–30. https://doi.org/10.1016/j.mfglet.2020.11.006
121. Ziwen CAO, Haiying XU, Shikun ZOU, Zhigang CHE (2012) Investigation of surface integrity on TC17 titanium alloy treated by square-spot laser shock peening. Chinese J Aeronaut 25:650–656
122. Liao Y, Cheng GJ (2013) Controlled precipitation by thermal engineered laser shock peening and its effect on dislocation pinning: multiscale dislocation dynamics simulation and experiments. Acta Mater 61:1957–1967. https://doi.org/10.1016/j.actamat.2012.12.016
123. Lainé SJ, Knowles KM, Doorbar PJ et al (2017) Microstructural characterisation of metallic shot peened and laser shock peened Ti–6Al–4V. Acta Mater 123:350–361. https://doi.org/10.1016/j.actamat.2016.10.044
124. Ye C, Suslov S, Fei X, Cheng GJ (2011) Bimodal nanocrystallization of NiTi shape memory alloy by laser shock peening and post-deformation annealing. Acta Mater 59:7219–7227. https://doi.org/10.1016/j.actamat.2011.07.070
125. Lu HF, Luo KY, Wu LJ et al (2019) Effects of service temperature on tensile properties and microstructural evolution of CP titanium subjected to laser shock peening. J Alloys Compd 770:732–741. https://doi.org/10.1016/j.jallcom.2018.08.161
126. Chattopadhyay A, Muvvala G, Sarkar S et al (2021) Effect of laser shock peening on microstructural, mechanical and corrosion properties of laser beam welded commercially pure titanium. Opt Laser Technol 133:106527
127. Pan X, He W, Huang X et al (2021) Plastic deformation behavior of titanium alloy by warm laser shock peening: Microstructure evolution and mechanical properties. Surf Coatings Technol 405:126670. https://doi.org/10.1016/j.surfcoat.2020.126670
128. Yong WANG, Xiaoyu PAN, Xibin WANG, Zhibing LIU, Shuyao LIU, Wenjuan WAN, Puyi WANG (2021) Influence of laser shock peening on surface integrity and tensile property of high strength low alloy steel. Chinese Journal of Aeronautics, 34(6), pp.199–208. J Aeronaut 36:199–208
129. Wang P, Cao Q, Liu S, Peng Q (2021) Surface strengthening of stainless steels by nondestructive laser peening. Mater Des 205:109754. https://doi.org/10.1016/j.matdes.2021.109754
130. Lu Y, Sun GF, Wang ZD et al (2020) The effects of laser peening on laser additive manufactured 316L steel. Int J Adv Manuf Technol 107:2239–2249
131. Wu J, Che Z, Zou S et al (2020) Surface integrity of TA19 notched simulated blades with laser shock peening and its effect on fatigue strength. J Mater Eng Perform 29:5184–5194
132. Yang Y, Lian X, Zhou K, Li G (2019) Effects of laser shock peening on microstructures and properties of 2195 Al-Li alloy. J Alloys Compd 781:330–336. https://doi.org/10.1016/j.jallcom.2018.12.118
133. Petronić S, Čolić K, Đorđević B et al (2020) Effect of laser shock peening with and without protective coating on the microstructure and mechanical properties of Ti-alloy. Opt Lasers Eng 129:106052
134. Wang H, Kalchev Y, Wang H et al (2020) Surface modification of NiTi alloy by ultrashort pulsed laser shock peening. Surf Coatings Technol 394:125899
135. Zhang H, Cai Z, Wan Z et al (2020) Microstructure and mechanical properties of laser shock peened 38CrSi steel. Mater Sci Eng A 788:139486. https://doi.org/10.1016/j.msea.2020.139486
136. Wang JT, Xie L, Wang ZG et al (2020) Influence of laser shock peening on the coefficient of thermal expansion of Al (7075)-based hybrid composites. J Alloys Compd 844:156088. https://doi.org/10.1016/j.jallcom.2020.156088
137. Trdan U, Skarba M, Grum J (2014) Laser shock peening effect on the dislocation transitions and grain refinement of Al–Mg–Si alloy. Mater Charact 97:57–68
138. Ren Y, Wan H, Chen Y et al (2021) Effect of laser shock peening and carbonitriding on tribological properties of 20Cr2Mn2Mo steel alloy under dry sliding conditions. Surf Coatings Technol 417:127215. https://doi.org/10.1016/j.surfcoat.2021.127215
139. Kubásek J, Molnárová O, Čapek J et al (2021) Laser shock peening of copper poly-and single crystals. Mater Charact 174:111037
140. Pan X, Guo S, Tian Z et al (2021) Fatigue performance improvement of laser shock peened hole on powder metallurgy Ni-based superalloy labyrinth disc. Surf Coatings Technol 409:126829. https://doi.org/10.1016/j.surfcoat.2021.126829
141. Wan Z, Guo W, Jia Q et al (2021) Effects of laser shock peening on microstructure and mechanical properties of TIG welded alloy 600 joints. Mater Sci Eng A 808:140914. https://doi.org/10.1016/j.msea.2021.140914
142. Sadeh S, Malik A (2021) Investigation into the effects of laser shock peening as a post treatment to laser impact welding. Mater Des 205:109701
143. Li W, Chen H, Huang W et al (2021) Effect of laser shock peening on high cycle fatigue properties of aluminized AISI

321 stainless steel. Int J Fatigue 147:106180. https://doi.org/10.1016/j.ijfatigue.2021.106180
144. Li J, Zhou J, Liu L et al (2021) High-cycle bending fatigue behavior of TC6 titanium alloy subjected to laser shock peening assisted by cryogenic temperature. Surf Coatings Technol 409:126848. https://doi.org/10.1016/j.surfcoat.2021.126848
145. Jiang W, Luo Y, Wang H, Wang BY (2015) Effect of impact pressure on reducing the weld residual stress by water jet peening in repair weld to 304 stainless steel clad plate. J Press Vessel Technol 137(3). https://doi.org/10.1115/1.4029655
146. Zelenak M, Foldyna J, Scucka J et al (2015) Visualisation and measurement of high-speed pulsating and continuous water jets. Measurement 72:1–8. https://doi.org/10.1016/j.measurement.2015.04.022
147. Mochizuki M, Enomoto K, Sakata S et al (1993) A study on residual stress improvement by water jet peening. In: Proceedings of the 5th International Conference on Shot Peening. pp 247–256
148. Kunaporn S, Chillman A, Ramulu M, Hashish M (2008) Effect of waterjet formation on surface preparation and profiling of aluminum alloy. Wear 265:176–185. https://doi.org/10.1016/j.wear.2007.09.008
149. Oka YI, Mihara S, Miyata H (2007) Effective parameters for erosion caused by water droplet impingement and applications to surface treatment technology. Wear 263:386–394. https://doi.org/10.1016/j.wear.2006.11.022
150. Srivastava M, Tripathi R, Hloch S et al (2016) Potential of using water jet peening as a surface treatment process for welded joints. Procedia Eng 149:472–480. https://doi.org/10.1016/j.proeng.2016.06.694
151. Kumar R, Chattopadhyaya S, Dixit AR et al (2017) Surface integrity analysis of abrasive water jet-cut surfaces of friction stir welded joints. Int J Adv Manuf Technol 88:1687–1701
152. Hassan AI, Chen C, Kovacevic R (2004) On-line monitoring of depth of cut in AWJ cutting. Int J Mach Tools Manuf 44:595–605. https://doi.org/10.1016/j.ijmachtools.2003.12.002
153. Mahmoudi AH, Jamali AM, Salahi F, Khajeian A (2020) Effects of water jet peening on residual stresses, roughness, and fatigue. Surf Eng 1–10. https://doi.org/10.1080/02670844.2020.1850196
154. Tönshoff HK, Kroos F, Marzenell C (1997) High-pressure water peening-a new mechanical surface-strengthening process. CIRP Ann 46:113–116. https://doi.org/10.1016/s0007-8506(07)60787-2
155. Barriuso S, Lieblich M, Multigner M et al (2011) Roughening of metallic biomaterials by abrasiveless waterjet peening: characterization and viability. Wear 270:634–639
156. Selvan MCP, Raju NMS (2012) Analysis of surface roughness in abrasive waterjet cutting of cast iron. Int J Sci Environ Technol 1:174–182
157. Azhari A, Schindler C, Li B (2012) Effect of waterjet peening on aluminum alloy 5005. Int J Adv Manuf Technol 67:785–795. https://doi.org/10.1007/s00170-012-4522-4
158. Xie J, Rittel D (2018) The effects of waterjet peening on a random-topography metallic implant surface. Eur J Mech 71:235–244
159. Azhari A, Schindler C, Hilbert K et al (2014) Influence of waterjet peening and smoothing on the material surface and properties of stainless steel 304. Surf Coatings Technol 258:1176–1182. https://doi.org/10.1016/j.surfcoat.2014.07.013
160. Azhari A, Schindler C, Godard C et al (2016) Effect of multiple passes treatment in waterjet peening on fatigue performance. Appl Surf Sci 388:468–474
161. Ma Y, Zhang Y, Liu J et al (2020) Hard milling of carburized and waterjet peened 18CrNiMo7-6 steel. Mach Sci Technol 25:288–306. https://doi.org/10.1080/10910344.2020.1815041
162. Balaji DS, Jeyapoovan T (2021) Multi-objective optimization in abrasive water jet peening on AA6063 alloy. Mater Today Proc 45:1928–1933. https://doi.org/10.1016/j.matpr.2020.09.220
163. Rivero A, Alberdi A, Artaza T et al (2018) Surface properties and fatigue failure analysis of alloy 718 surfaces milled by abrasive and plain waterjet. Int J Adv Manuf Technol 94:2929–2938
164. Balamurugan K, Uthayakumar M, Gowthaman S, Pandurangan R (2018) A study on the compressive residual stress due to water jet cavitation peening. Eng Fail Anal 92:268–277. https://doi.org/10.1016/j.engfailanal.2018.05.012
165. Srivastava AK, Nag A, Dixit AR et al (2017) Surface integrity in tangential turning of hybrid MMC A359/B 4 C/Al 2 O 3 by abrasive waterjet. J Manuf Process 28:11–20. https://doi.org/10.1016/j.jmapro.2017.05.017
166. den Dunnen S, Mulder L, Kerkhoffs GMMJ et al (2013) Waterjet drilling in porcine bone: the effect of the nozzle diameter and bone architecture on the hole dimensions. J Mech Behav Biomed Mater 27:84–93. https://doi.org/10.1016/j.jmbbm.2013.06.012
167. Muruganandhan R, Mugilvalavan M, Thirumavalavan K, Yuvaraj N (2017) Investigation of water jet peening process parameters on AL6061-T6. Surf Eng 34:330–340. https://doi.org/10.1080/02670844.2017.1394564
168. He Z, Yu H, Zhao S et al (2020) An experimental and numerical analysis of water jet peening of Al6061-T6. Int J Adv Manuf Technol 107:3833–3845. https://doi.org/10.1007/s00170-020-05282-1
169. Sadasivam B, Hizal A, Arola D (2009) Abrasive waterjet peening with elastic prestress: a parametric evaluation. Int J Mach Tools Manuf 49:134–141. https://doi.org/10.1016/j.ijmachtools.2008.10.001
170. Azhari A, Schindler C, Nkoumbou J, Kerscher E (2014) Surface erosion of carbon steel 1045 during waterjet peening. J Mater Eng Perform 23:1870–1880. https://doi.org/10.1007/s11665-014-0932-9
171. Sekyi-Ansah J, Wang Y, Quaisie JK et al (2020) Surface characteristics and cavitation damage in 8090Al–Li alloy by using cavitation water jet peening processing. Iran J Sci Technol Trans Mech Eng 45:299–309. https://doi.org/10.1007/s40997-020-00401-5
172. El-Banna A, Bissa MW, Khurshid Z et al (2020) 4—Surface modification techniques of dental implants. Dent Implant Woodhead Publ Duxford, UK 49–68
173. Liu X, Liu J, Zuo Z, Zhang H (2019) Effects of shot peening on fretting fatigue crack initiation behavior. Mater (Basel, Switzerland) 12:743. https://doi.org/10.3390/ma12050743
174. Ismail S, Ahsan Q, Haseeb ASMA (2017) 2.7 recent advances in mechanical surface treatment 171–179
175. Antunes RA, de Oliveira MCL (2015) Effect of surface treatments on the fatigue life of magnesium and its alloys for biomedical applications. In Surface modification of magnesium and its alloys for biomedical applications (pp. 283–310). Woodhead Publishing.
176. Karthik D, Yazar KU, Bisht A, Swaroop S, Srivastava C, Suwas S (2019) Gradient plastic strain accommodation and nanotwinning in multi-pass laser shock peened 321 steel. Appl Surf Sci 487:426–432
177. Zhou L, Li Y, He W, He G, Nie X, Chen D, An Z (2013) Deforming TC6 titanium alloys at ultrahigh strain rates during multiple laser shock peening. Mater Sci Eng A 578:181–186
178. Mardi KB, Dixit AR, Pramanik A, Hvizdos P, Mallick A, Nag A, Hloch S (2021) Surface topography analysis of mg-based composites with different nanoparticle contents disintegrated using abrasive water jet. Materials 14(19):5471
179. Ding X, Kang Y, Li D, Wang X, Zeng D (2017) Experimental investigation on surface quality processed by self-excited oscillation pulsed waterjet peening. Materials 10(9):989